MARMARA UNIVERSITY
INSTITUTE FOR GRADUATE STUDIES IN PURE AND APPLIED SCIENCES

THE SYNTHESIS OF CLAY-POLYMER COMPOSITE ABSORBENTS FOR OIL REMOVAL FROM AQUEOUS SOURCES

SİNEM ABALI

MASTER THESIS
Department of Chemical Engineering

Thesis Supervisor
Asst. Prof. Yaşar Andelib AYDIN

ISTANBUL, 2020

MARMARA UNIVERSITY
INSTITUTE FOR GRADUATE STUDIES IN PURE AND APPLIED SCIENCES

THE SYNTHESIS OF CLAY-POLYMER COMPOSITE ABSORBENTS FOR OIL REMOVAL FROM AQUEOUS SOURCES

SİNEM ABALI

(524517014)

MASTER THESIS
Department of Chemical Engineering

Thesis Supervisor
Asst. Prof. Yaşar Andelib AYDIN

ISTANBUL, 2020

ACKNOWLEDGMENT

First of all, I would like to express my sincere thankfulness to my master thesis advisor, Asst. Prof. Yaşar Andelib AYDIN, for her valuable guidance, endless support, understanding and encouragement throughout my thesis study. It has been a great honor to work with her.

I would like to thank Prof. Dr. Atıf KOCA and Prof. Dr. Fatma KARACA in the Department of Chemical Engineering for giving me opportunity to use high pressure reactor, Prof. Dr. Münir TAŞDEMİR in the Department of Metallurgical and Materials of Technology Faculty for allowing to use twin-screw extruder, and Asst. Prof. Gülşen ALBAYRAK ARI in the Department of Chemical Engineering of İstanbul University for providing me to use hot press machine.

I would also like to thank Marmara University Faculty of Engineering for offering me the opportunity to carry out my thesis and Marmara University Scientific Research Project Coordination Unit (BAPKO) for the financial support.

And finally, I would like to thank my family who supported and encouraged me all my life.

December, 2020 **Sinem ABALI**

TABLE OF CONTENTS

ÖZET

SU KAYNAKLARINDAN YAĞ GİDERİMİ İÇİN KİL POLİMER KOMPOZİT ABSORBANLARIN SENTEZİ

Su kaynakları, sucul yaşam için büyük bir tehdit olan yağlarla sürekli olarak kirlenmektedir. Bu nedenle, dökülen yağlar etkili bir temizleme yöntemi kullanılarak sudan uzaklaştırılmalıdır. Polimer esaslı köpükler, hafif, yüksek gözenekli ve esnek yapıları nedeniyle yağ emici malzeme olarak sıklıkla kullanılmaktadır.

Bu tezde, LDPE-organosepiyolit kompozit köpükler yağ emici malzemeler olarak sentezlenmiştir. Bu amaçla, Eskişehir sepiyoliti değişen reaksiyon koşulları altında trimetoksi(oktadesil)silan, (3-glisidiloksipropil)trimetoksisilan ve (3-aminopropil)trietoksisilan ile organik modifikasyondan önce saflaştırılmış ve asitle muamele edilmiştir. Sentezlenen sepiyolit numuneleri yağ absorpsiyon testlerine tabi tutulmuş, ve BET, TGA ve FT-IR analizleri ile karakterize edilmiştir. En oleofilik sepiyolit, kompozit malzeme sentezi için dolgu maddesi olarak seçilmiştir. Ağırlıkça, %5, %10 ve %20 organosepiyolit içeren LDPE-organosepiyolit kompozit pelletleri eriyik karıştırma ile çift vidalı ekstrüder kullanılarak üretilmiş ve sonra plaka formuna getirilmiştir. Plakalar, yığın köpürtme ile köpürtme ajanı olarak CO_2 kullanılarak 45, 70 ve 110 bar doyma basınçlarında köpürtülmüştür. Sentezlenen köpüklerin absorpsiyon kapasitesi zeytinyağı, atık zeytinyağı, motorin ve benzin için belirlenmiştir. Yeniden kullanılabilirlik özelliği de ayrıca araştırılmıştır. Köpük morfolojileri SEM ile analiz edilmiştir.

Sonuçlara göre, asitle muamele edilmiş sepiolit, muamele edilmemiş sepiolite göre daha verimli bir şekilde silillenmiştir. (3-glisidiloksipropil) trimetoksisilan ile modifiye edilmiş sepiolit, kompozit köpükler için dolgu maddesi olarak seçilmiştir. En yüksek yağ emme kapasitesi (3,38 g/g) ve hacim genleşme oranı (7,43), 70 barda doymuş ağırlıkça % 10 organosepiyolit içeren köpük ile elde edilmiştir. Sonuç olarak, sentezlenmiş LDPE-organosepiyolit kompozit köpükler, su ortamından yağı verimli bir şekilde uzaklaştırabilir.

ABSTRACT

THE SYNTHESIS OF CLAY-POLYMER COMPOSITE ABSORBENTS FOR OIL REMOVAL FROM AQUEOUS SOURCES

Aqueous sources are continuously polluted with oils which is a greatly threat to aquatic life. Therefore, spilled oils must be removed from water using an efficient cleaning method. Polymer based foams are frequently used as oil absorbent materials due to their lightweight, highly porous and flexible structure.

In this thesis, LDPE-organosepiolite composite foams were synthesized as oil absorbent materials. For this purpose, Eskişehir sepiolite was purified and acid treated prior to organic modification using trimethoxy(octadecyl)silane, (3-glycidyloxypropyl)trimethoxysilane and (3-aminopropyl)triethoxysilane under varying reaction conditions. The synthesized sepiolite samples were subjected to oil absorption tests and characterized with BET, TGA and FT-IR analysis. The most oleophilic sepiolite was selected as filler for composite material synthesize. LDPE-organosepiolite composite pellets containing 5%, 10 % and 20% (w.) organosepiolite were produced by melt mixing using a twin screw extruder and then formed into sheets. The sheets were foamed by batch foaming using CO_2 as foaming agent at saturation pressures of 45, 70 and 110 bar. The absorption capacites of synthesized foams were determined for olive oil, waste olive oil, diesel and gasoline. The reusability feature was also investigated. Foam morphologies were analyzed with SEM. According to the results, acid-treated sepiolite was more efficiently silylated than untreated sepiolite. (3-glycidyloxypropyl)trimethoxysilane modified sepiolite was selected as the filler for composite foams. The highest oil absorption capacity (3.38 g/g) and volume expansion ratio (7.43) was obtained with the foam containing 10 % (w.) organosepiolite saturated at 70 bar. Consequently, synthesized LDPE-organosepiolite composite foams can remove oil from aqueous media efficiently.

SYMBOLS

cm **:** Centimeter

°C **:** Degree Celsius

g **:** Gram

h **:** Hour

m **:** Meter

mm **:** Milimeter

ml **:** Mililiter

µL **:** Microliter

µm **:** Micrometer

min **:** Minute

M **:** Molarity

rpm **:** Round per minute

ABBREVIATIONS

APTES **:** (3-aminopropyl)triethoxysilane

ASEP **:** Acid treated sepiolite

BET **:** Brunauer-Emmett-Teller

DTG **:** Differential thermogravimetry

FTIR **:** Fourier-transform infrared spectroscopy

GPTMS **:** (3-glycidyloxypropyl)trimethoxysilane

SEM **:** Scanning electron microscope

SEP **:** Pre-treated sepiolite

TGA **:** Thermogravimetric analysis

TMODS **:** Trimethoxy(octadecyl)silane

XRD **:** X-ray diffraction

LIST OF FIGURES

LIST OF TABLES

1. INTRODUCTION

Among natural resources, water is the most fundamental requirement for all living things to continue their vital activities. Water is an irreplaceable natural resource needed in all areas of life such as agriculture, energy production, industry, daily household activities, etc. The availability of adequate and uncontaminated water is essential to food and energy production, industrial development as well as the future of humanity and other lives [1].

Continuous increase in world population and rapid development of technology leads to increase in water usage areas and amounts. This situation reduces the water quality continuously and indicates that the need for clean water will gradually increase [2]. Some of the major reasons of water pollution are discharges of untreated industrial and municipal wastewaters [3], sea based activities, usage of toxic chemicals in agriculture, garbage thrown into the water, etc [2].

1.1. Overview of Oil Spill Occurrences to Aqueous Sources

There are a wide variety of oils in the water environment, such as crude oil, refined products (light and heavy fuels), machine oils, edible oils (vegetable and animal oils), etc [4]. These various types of oils can reach water resources in many miscellaneous ways. In general, petroleum pass to the water environment from exploration, production, transportation and consumption related spills, natural oil leakages, operational oily waste discharges left by ships and tankers, oil refineries and other untreated industrial wastewaters and even wars [5]. Edible oils enter the aquatic environment by discharging untreated urban wastewater into seas [6].

Today, petroleum is a crucial important energy source. Worldwide, oil transportation is usually carried out by sea. However, oil transport by sea carries a high risk of oil spills caused by tanker accidents [7]. To date, numerous large (more than 700 tonnes), medium (between 7 and 700 tonnes) and small (less than 7 tonnes) scale oil spills have occurred worldwide as a result of tanker accidents. As shown in the Figure 1.1 and Figure 1.2, between 1970 and 2018, approximately 5.86 million tonnes of oil entered to the water environment. Between 1970 and 1979, 245 large scale and 543 medium scale oil spills occurred and approximately 3,195,000 tons of oil were spilled into sea. The

number of tanker accidents and the quantity of spilled oil have decreased continuously with each passing decade. Between 2010 and 2018, only 17 large scale and 42 medium scale oil spills occurred, and approximately 163,000 tons of oil spilled into the sea [8].

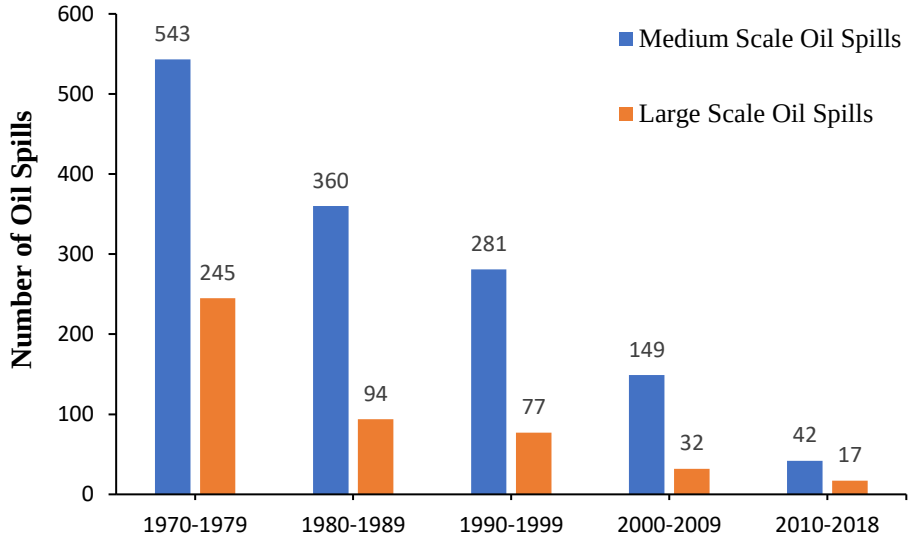

Figure 1.1. The number of medium and large oil spills caused by tanker accidents around the world per decade from 1970 to 2018 [8].

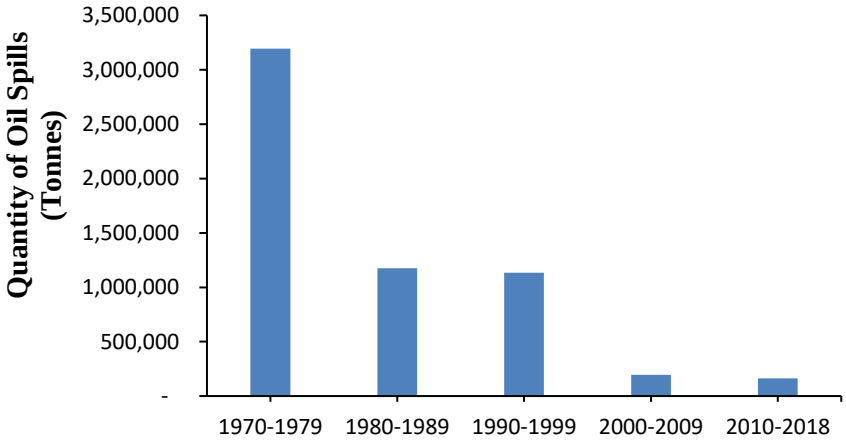

Figure 1.2. The quantity of all oil spills caused by tanker accidents around the world per decade from 1970 to 2018 [8].

Although there is a noticeable reduction in the number and quantity of oil spills, there is always a risk that the accidents will occur at any time. More recently, three large scale oil spills occurred in China, the East China Sea and the Persian Gulf, and three medium

scale oil spills in the Gulf of Guinea, Europe and Africa in 2018. The oil spill occurred in the East China Sea, 116,000 tonnes of oil passed into the sea. This has been the largest oil spill due to the tanker accident in the last 24 years [8].

The Sea of Marmara, İstanbul and Çanakkale Strait are important oil transport routes that serve as a bridge between the continents of Europe and Asia. Every day a large number of loaded tankers passing through these areas are at risk of oil spill accidents. To date, many tanker accidents have occurred in the Sea of Marmara. Between 1960 and 2010, quantities of oil ranging from 10 tons to 95,000 tons were poured into the Sea of Marmara, due to various tanker accidents. The cleaning operations of the spilled oil took months or even years depending on the quantity and quality of the oil, the efficiency of the equipment used, the sea and weather conditions [9].

Other significant occurrence of oil spills is submarine petroleum and natural gas reservoirs that leak out of the ground of sea. According to GESAMP technical report (2007), the rate of total natural leakages into aqueous sources ranged from 0.2 to 2 million tons per year all over the world [5].

Oil spills in water sources are environmental disasters that cause great damages to marine life, fishing and marine industry, some social and economic activities. Due to causing the chemical toxicity in the aquatic environment, oil spills may result in poisoning or death of fish, seabirds, marine mammals and other aquatic creatures depending on the quantity and quality of the oil spills [10]. Fishing and mariculture are one of the most affected industries from oil spills [11]. Besides that, tourism sector negatively affects from oil spills due to oil contaminated inshore waters and shorelines. Moreover, if the spilt oil cannot be recovered, it causes great economic losses [12].

Microbial degradation rate of oil in nature is very low. Therefore, if an oil leak is not immediately intervened, this oil undergoes a series of weathering processes until it is degraded and maintains its presence in the water for a long time [6]. Since most oils have relatively lower density than sea water, the leaked oil floats on the surface of the water and spreads quickly depending on sea conditions and wind [13]. After an oil spill occurs, the weathering process briefly takes place as follows:

- The volatile components that have low boiling points in the oil, evaporate within the first 24 hours.

- Soon after the spill, the water-soluble components in the oil begin to dissolve and create toxic effects for water ecosystems.
- Oil-water emulsions are formed when water droplets penetrate the oil layer.
- Small oil droplets disperse and spread in water environment.
- For the spreading oil droplets, biodegradation proceeds very slowly.
- Oil components with higher density than water, sink to the sea bottom and forms tar globs at low temperatures [14].

As the weathering processes progress, it becomes increasingly hard to remove oil. For this reason, the oil spilled area must be cleaned using a suitable cleaning method without wasting time and the spilled oil must be recovered as high as possible [15].

1.2. Techniques of Oil Removal from Aqueous Sources

Today, there are many techniques used to clean oil from aqueous sources. Some of them can only remove oil from water without recovery, while others can both remove oil from water and recover it. While some of these methods may be used alone, the use of several techniques together can provide higher cleaning rates and effectiveness. The most commonly used methods, namely, booms, skimmers, dispersants, in-situ burning, bioremediation and oil sorbents are described as follows.

1.2.1. Booms

Booms, also called as floating barriers restrict spilled oil in a certain area to prevent spreading over the water surface and concentrate the oil to ease recovery. They are available in various types, sizes, lengths and materials to offer solutions for different conditions. The common types of booms are curtain, fence, shore sealing and fire-resistant booms. An ideal boom must be buoyant and durable to the sea and weather conditions [13,16]. Booms can be used for all types of oil. However, there are some disadvantages of this technique. Booms are expensive and complex equipment. They require extensive labour with large equipment and require a great number of employees [9,13].

1.2.2. Skimmers

Skimmers are mechanical devices that can be used together with booms to remove the oil slick from the surface of water. Skimmers don't modify the chemical properties of oil, thus the recovered oil can be reused after further treatment. There are various skimmers produced from oleophilic or non-oleophilic materials. The efficiency of skimmers depends on weather and sea conditions, the viscosity of the oil and pump capacity of the skimmer. Skimmers are expensive and complex devices and collecting oil requires extensive labour [13,17].

1.2.3. Dispersants

Dispersants are chemicals obtained by dissolving the surfactants in one or several solvents. They are applied by spraying to the oily area. Dispersants are soap-like molecules [18], that consist of two parts, hydrophilic and oleophilic. The hydrophilic part of the dispersants adheres to water and the oleophilic part adheres to the oil [9]. Thus, they allow the oil to be mixed into the water in small droplets and this accelerates the microbial degradation. However, most dispersants have a toxic effect in the aquatic environment, damaging human health and aquatic life. In addition, since the spilled oil is removed from the environment by degradation, oil recovery is not possible [13].

1.2.4. In-situ burning

In the in-situ burning technique, oil layer present on water surface is removed by burning with the help of an igniter. In order to achieve effective combustion, the oil layer thickness must be at least 2-3 mm to prevent heat lost to the sea [18]. This method can be effective when applied just after the spill in calm weather conditions**.** As a result, large amounts of fume are produced. The composition of the fume is dependent upon oil type. However, major components can be listed as carbon monoxide, carbon dioxide, sulfur dioxide, nitrogen oxides and volatile organics. The residue from burned oil may create toxic effect on water environment. Moreover, oil cannot be recovered by this method [13].

1.2.5. Bioremediation

Oil removal by bioremediation method is based on biodegradation of oil through hydrocarbon-degrader microorganisms like bacteria and fungi. The technique may be applied either by introducing nutrients into the medium to allow growth of microorganisms already present in the water environment or by introducing new microorganisms into the medium to increase the rate of degradation process [18]. The efficiency of the technique depends on adequate amount of nutrients, dissolved oxygen and temperature conditions in the environment [13]. This technique is generally preferred, if weathering process has advanced [9]. Also, with this technique, it is not possible to recover oil.

1.2.6. Oil sorbents

In this technique, the sorbent is applied to the oily area and waited for sorption of oil. After the oil sorption is completed, the used sorbent is removed from the site and if the material is suitable for multiple uses, it is squeezed under a certain pressure to recover the sorbed oil and can be used repeatedly [18]. Unlike other methods, it is possible for an ideal oil sorbent to remove and recover overall oil from the water [19].

Oil sorbents are hydrophobic and oleophilic materials that remove oil from water environment by way of adsorption and/or absorption mechanism. Adsorption involves only adherence of oil molecules to the surface of the sorbent material called as adsorbent. On the other hand, absorption is based on diffusion of oil into the voids in the structure of the sorbent material called as absorbent [20]. The term of sorption encompass both of adsorption and absorption [21]. There are a number of features that characterize an ideal oil absorbent as follows:

- Hydrophobicity and oleophilicity are the most significant requirements for an oil absorbent. The material that used to absorb oil from the aquatic medium must have a high affinity to oil (oleophilicity), and be able to repel water (hydrophobicity) [22]. Otherwise, an absorbent that is not sufficiently hydrophobic may also absorb water besides oil [23].
- The material of an oil absorbent must have high surface area [24]. The increment in surface area improves absorption capacity of the material. [23].

- The structure of the material should have high porosity. The porous structure eases penetration of oil into the structure of the absorbent [24].
- Buoyancy is an another important property that affect absorption performance of the material [23]. An absorbent must remain afloat to effectively remove oil slicks on the surface of water.
- The absorbent material must be able to retain the absorbed oil as long as possible**.**
- It should be durable to sea and weather conditions [22].

In literature, it has been observed that the studies mainly focus on three material groups as oil sorbent i.e. natural organics, synthetic organics and natural inorganics. A broad array of natural organic sorbents have been reported include cotton [25-28], corncobs [29], baggase, rice hull [12], walnut shell [30], kapok [31], milkweed floos, kenaf [28], raw luffa [32], sawdust [33], etc. These materials are cheap and readily available [13]. However, the absorbents constructed from natural organics initially have high buoyancy, but they can not remain afloat as time progress and ultimately sink [22]. Thus, after their use the collection of natural organics from water is a labor-intensive process [13]. Moreover, the absorbents are constructed from natural organic materials shows low oil absorption efficiency [34]. The examples of synthetic organic sorbents reported in the literature can be listed as polyethylene film [35], polypropylene foam [36]**,** polyurethane foam [37], butyl rubber [38], polyvinyl chloride [25], polyacrylonitrile [39], waste tire powder [40], etc. The main disadvantage of synthetic organics is that they are non-biodegradable materials [13]. Some of the reported synthetic organic sorbents can be listed as sepiolite [41,42], bentonite [43], vermiculite [4], expanded perlite [44], activated carbon [45], exfoliated graphite [46], etc.

1.3. Clay Minerals

Clay minerals are classified mainly as natural and synthetic clay minerals. Natural clay deposits that are stacked silicates containing some impurities, are gradually produced by the effect of weathering processes. On the contrary, synthetic ones are pure materials that are obtained in a short time [47].

Clays are a member of phyllosilicates also known as layered silicates. Each layer is composed of tetrahedral and octahedral sheets. Tetrahedral sheets comprise of tetrahedrons containing one silicon or aluminium connected with four oxygen atoms. Octahedral sheets comprise of octahedrons containing one aluminium, magnesium or iron atom connected with six O atoms or hydroxyls [48] Generally, the structure of clays is formed from 1:1, 2:1 or 2:1:1 type clay mineral layer. 1:1 (two sheet phyllosilicates) type layer consist of linking of one tetrahedral and one octahedral sheet (Figure 1.3a). In 2:1 (three sheet phyllosilicates) type layer, an octahedral sheet is placed between two tetrahedral sheets (Figure 1.3b) [49]. Apart from these two types, 2:1:1 (four sheet phyllosilicates) type layer shows extremely different compositions [47].

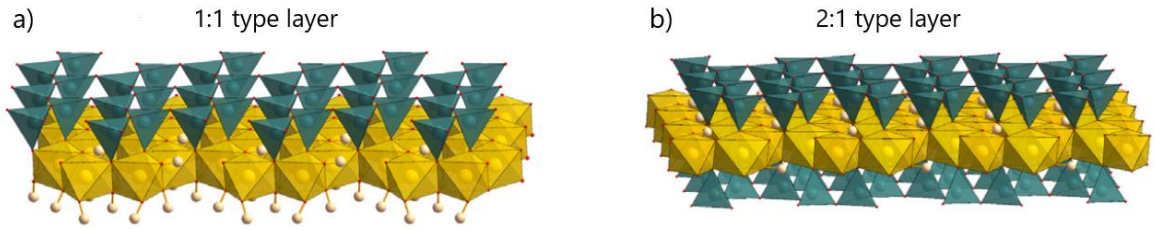

Figure 1.3. (a) 1:1 and (b) 2:1 type clay mineral layers [48]

Clays may be categorized into seven groups as (i) kaolinite and serpentine, (ii) micas, (iii) vermiculite, (iv) smectites, (v) pyrophyllite and talc, (vi) chlorites and (vii) palygorskite and sepiolite [49].

1.3.1. Overview of sepiolite

Sepiolite is a fibrous clay found in the palygorskite and sepiolite group of clay minerals [49]. Sepiolite is generally formed by hydrothermal alteration or precipitated in environment. The deposits of sepiolite is guessed as 8000 million tonnes in worldwide. Spain has the largest sepiolite reserves over 3800 million tonnes [50]. The other sepiolite deposits are mostly existed in the Turkey, South Africa, Argentina, United States, China, etc. Turkey has rich sepiolite deposits especially found in Western and Central regions of Anatolian [51].

1.3.1.1. Chemical structure of sepiolite

Sepiolite is a modulated fibrous phyllosilicate. The theorical half unit-cell formula of sepiolite is $Si_{12}O_{30}Mg_8(OH)_4(OH_2)_4.8H_2O$. The crystal structure is constituted by the alternation of 2:1 type layers and tunnels that extend throughout the fibers. Each layer is composed from a magnesium oxide-hydroxide octahedral sheet between two silica tetrahedral sheets (Figure 1.4) [52].

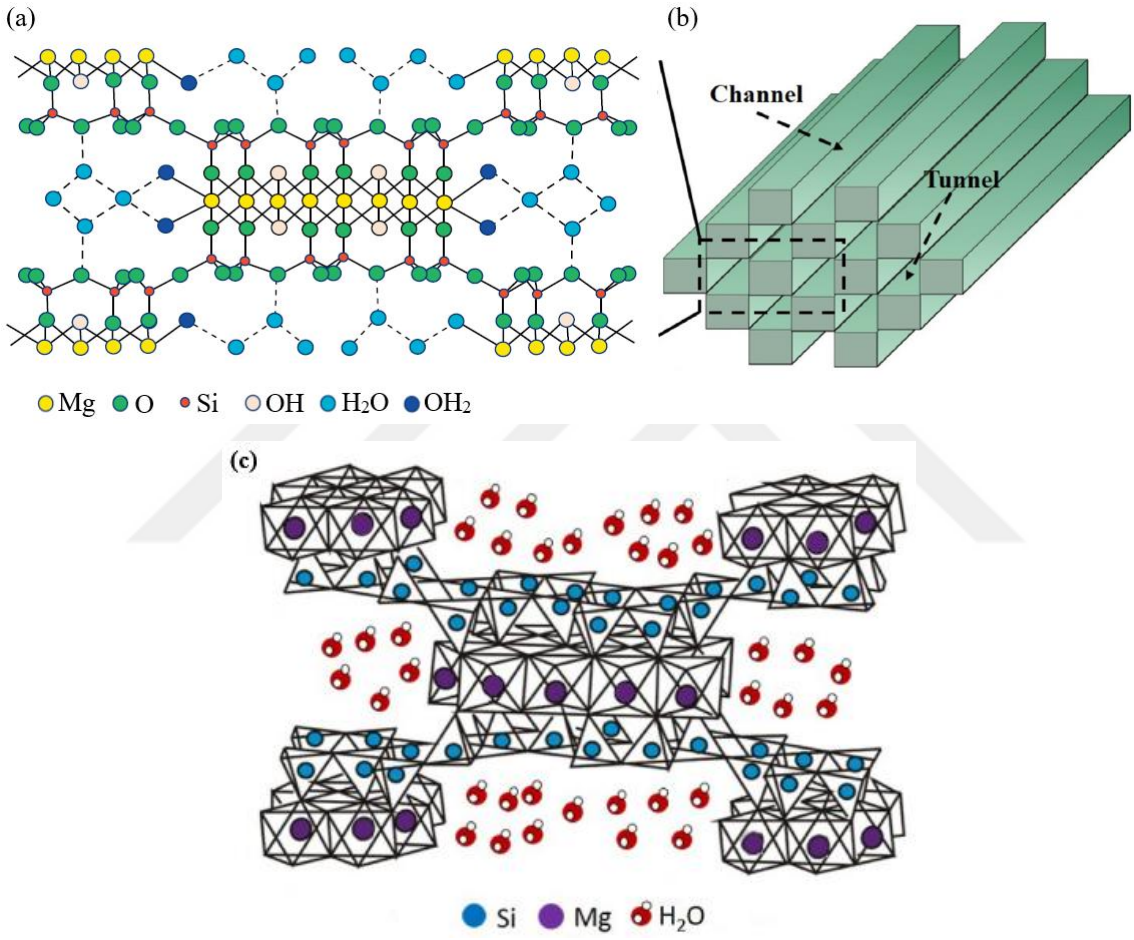

Figure 1.4. (a) The crystal structure of sepiolite with atoms and molecules [53] (b) fibrous structure of sepiolite [54], (c) the crystal structure of sepiolite with the tetrahedral and the octahedral sheets [54].

In the structure of sepiolite, the silica tetrahedrons are extended continuously like other ideal 2:1 types of phyllosilicates. But, apical oxygen atom of the tetrahedrons turns down every six units. This inversion causes discontinuity of octahedral sheets that differs sepiolite from other ideal 2:1 type of phyllosilicates, therefore it is called as a

modulated phyllosilicate. The discontinuity results in formation of rectangular shaped tunnel voids within the crystal structure. Structural channels are often generated by breaking of the octahedral sheets and extend parallel to fibre axis. The fibrous morphology and the cavities in the structure leads to high porosity and surface area which provide sepiolite a high capacity for sorption of voluminous organic molecules [47,51,55].

Water is present in sepiolite structure in adsorbed, zeolitic and coordinated state. Adsorbed water also known as hydroscopic water is present on the sepiolite surface and its quantity depends on the ambient humidity. Zeolitic water is found in the mineral channels [56]. Coordinated water molecules present on the edges of octahedral sheets to complete the octahedral coordination of Mg^{+2} cations [57]. Coordinated waters are also connected to the zeolitic water molecules with hydrogen bond [58]. Also, hydroxyl groups (-OH) are found at the center of the 2:1 layers of sepiolite and they leave from structure as structural water [59].

Theoretically, octahedral sheets of sepiolite consist Mg^{2+} as octahedral cations. However, it may be possible to partially replace of Mg^{2+} octahedral cations with Al^{3+} and/or Fe^{3+} during the formation of the mineral. This replacement causes the formation of negative charges and framework defects. Besides that, tetrahedral Si^{4+} cations may be replaced with Al^{3+}. Therefore, a significant amount of exchangeable cations are found in the channels of sepiolite fibers to compensate for these charge imbalances [50].

On the surface of the tetrahedral sheets of sepiolite, there is a large concentration of silanol groups (-SiOH) present only in 2:1 type of clay minerals [60]. These groups are naturally formed as a consequence of broken Si-O-Si bonds due to the discontinuity of octahedral sheets of sepiolite. The broken Si-O-Si bonds receive either H^+ or -OH group to neutralize their residual charge to form silanol groups [21]. These groups provide notable hydrophilic nature to the sepiolite [61]. Moreover, the silanol groups are capable to make covalent bond with some chemical reagents such as silanes. This feature can be used for organic modification of sepiolite surface [47].

1.3.1.2. Applications of sepiolite

Sepiolite is a special clay as due to its fibrous morphology, high surface area and active groups on its surface [50]. Therefore, sepiolite has been used in a broad range of industrial applications including wastewater treatment, oil spill clean-up, filler for polymers composites, industrial and floor absorbents, agricultural carrier, pharmaceuticals, moisture control, cosmetics, paints and coatings, pet litters, etc. [51].

1.4. Polymer composites

Polymer composites consist of at least a polymer as matrix phase and an inorganic material such as clay, carbon nanotube, metals and metal oxides, etc., as filler phase [62,63]. Polymers have many superior properties such as processability, light weight and flexibility, and this makes polymers useful in broad range applications. But they have low mechanical properties. Inorganic fillers are generally rigid and thermally stable materials. Composite technology offers to polymeric materials improved mechanical properties without alter their intrinsic features by combining the advantages of these two different materials [61,64].

The mechanical properties of the eventual composite material are highly depended on interface interactions between inorganic and organic phases, and the quality of dispersion of inorganic material in organic matrix phase [62]. Here, the term “interface” refers to a two-dimensional boundary between inorganic component and the organic polymer matrix. The high degree of interactions at interface leads to the formation of chemically or mechanically altered three-dimensional region which is called as “interphase” [65].

The particle size and aspect ratio of the used inorganic filler are other important factors which also effect the mechanical properties of the composite material. Nano size inorganic particles have higher surface area than micro size inorganic particles. Due to high aspect ratio, using nanoparticles significantly enhances the interfacial area which enables for higher interaction between the inorganic particles and the organic polymer matrix [61].

In the case of clay-polymer composites, they cannot be successfully synthesized by the incorporation of natural clay minerals and most of polymer matrices [64,66]. Natural

clay minerals tend to agglomerate due to their high surface area [67] and the strong van der Waals forces between their particles [62]. The formation of agglomerates adversely affects the dispersion of the clay and interphase properties by limitation of interphase area and interaction between the clay and polymer matrix [67]. Moreover, clays in raw form are inherently hydrophilic and they are not compatible with hydrophobic polymers. However, they can be incorporated into some hydrophilic polymers namely, poly(ethylene glycol), ,poly(vinyl alcohol) and poly(ethylene oxide) [68,69]. The intrinsic hydrophilicity of natural clay minerals hinders the dispersion of the clay layers within the polymer, which results in poor interfacial interactions between the clay and the polymer. This incompatibility also enhances the formation of clay agglomerates. Both insufficient dispersion of the clay in the polymeric matrix and poor interfacial interaction between the composite components causes generation of more heterogeneous composite material. All of these factors cause noticeable reduction in the eventual mechanical properties of the composite [62,67,70]. Therefore, it is crucial to generate strong repulsion between the clay particles to prevent their agglomeration and increase compatibility between clay particles and polymer matrix to improve interfacial interaction. In such cases, one of the most common method is the surface modification of clays using chemical reagents that improve the interfacial interaction and the dispersion of clay in hydrophobic polymer matrices [61,68,70,71].

With all factors in mind, fibrous clays may have processing advantages for synthesizing clay-polymer composites. They disaggregate more easily than typical plate shaped clays due to poor interactions arising from the relatively smaller contact area between fibers. As a fibrous clay mineral, sepiolite may be a good candidate as inorganic filler material to produce clay-polymer composite due to its high specific surface area and small aspect ratio [55,72]. When the proper surface treatment method is applied, sepiolite can be used as an inorganic filler in various hydrophobic polymer matrices [73].

1.5. Surface Modification Methods of Clay Minerals

The modification of clay surfaces is frequently used method for synthesizing hydrophilic clay-hydrophobic polymer composites. Surface modification attaches the hydrophobic characteristic to the hydrophilic clay surfaces.

The level of interaction between the organic and inorganic component ranges from durable chemical bonds to poor friction forces. Therefore, the characteristic of the interface interactions is crucial in stability of the composite material [74].

The hydrophobic groups can be attached to the clay surface either by chemical or physical modification methods. In the case of chemical modification methods, coupling agents and grafted polymers are generally used as modifier. The surface modification by chemical methods based on chemical interactions between modifiers and clay surfaces. Silane coupling agents are commonly used as coupling agent whose functional groups react with the silanol groups on the clay surfaces. In the case of physical methods, surfactants are generally used as modifier. The physical modification methods based on physical interactions between modifiers and clay surfaces. Quaternary alkyl ammonium salts and amines are commonly used as surfactants whose polar groups are adsorbed onto the clay surface through electrostatic interactions. Chemical modification methods provide much strong interaction between the modifiers and clay surfaces than physical modification methods due to the formation of durable covalent bonds [55,61].

Sepiolite in natural form is hydrophilic and it is not compatible with hydrophobic polymers. Therefore, modification of the hydrophilic surface of sepiolite is essential to improve the compatibility of this mineral with hydrophobic polymers. As mentioned earlier, sepiolite consists significant amount of silanol groups at the edges of its tetrahedral sheets and exchangeable cations in its channels. The silanol groups and exchangeable cations present in the structure of sepiolite can be used in order to modify the hydrophilic surface of the mineral [75]. In literature, many studies have been reported related to the organic modification of the surface of sepiolite. For this purpose, silane coupling agents [71,72,75] and quaternary ammonium salts [55,76] are mainly used. Raji et al. (2018) were synthesized clay-polymer nanocomposites using three separately clays, namely, sepiolite, montmorillonite and halloysite, and polypropylene (PP) as polymer matrix. They prepared the composites using the clay minerals in raw and organically modified (by silylation process) forms. They observed agglomerations in the raw clay-PP nanocomposites due to strong van der Waals forces between the raw clay fines, while they observed homogeneous clay dispersion in organomodified clay-PP nanocomposites [71]. As a result, organic modifiers improve interfacial adhesion between the clay and polymer constituents by creating more interphase space whose

presence positively affects the overall performance of the final composite [75]. Therefore, organic modification improves dispersion of clay fines in polymer and interface interactions between clay and polymer matrix.

1.5.1. Silylation

Silylation (also called as silanization or silane grafting) is commonly used process to organically modify the surface of inorganic materials [77]. In silylation, a covalent bond is formed between the silane coupling agents and the reactive hydroxyl groups on the clay surface. The silane coupling agents enables the placement of hydrophobic groups capable of reacting with hydrophobic polymers on the surface of the clay [49].

A silicon atom can stably form four single bonds. A silane molecule is constituted by bonding four identical or different substituents to a silicon atom (Figure 1.5). If, one of these substituents is an organic group which is directly binded to the silicon atom via silicon-carbon bond, this molecule is called as organosilane [78].

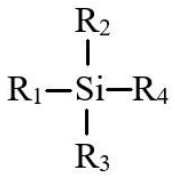

Figure 1.5. General chemical formula of a silane

Silane coupling agents are classified as organosilane compounds having generally three inorganic reactive groups and one organic group. The general structural formula of silane coupling agents is as follows:

$$R_xSi(OR')_{4-x} \quad (1.1)$$

Here in, "R" represents either a reactive organic group such as vinyl, mercapto, amino, methacrylate, etc. or an unreactive organic group such as alkyl, aryl, etc. "OR′" represents inorganic reactive groups that may be methoxy, ethoxy or hydroxyl [58,78]. The inorganic reactive groups can covalently bond with inorganic materials such as minerals, metals, glass fiber, etc. The organic reactive group reacts with organic materials such as, plastics, rubbers, coatings etc. Thus, the dual functionality of silane

coupling agents serves as a bridge between inorganic and organic materials and enhance miscibility of the two dissimilar materials (Figure 1.6) [78]. Many studies confirmed that, organomodification of various types of clay using organosilanes improved the wetting ability between polymer and clay [71,79,80].

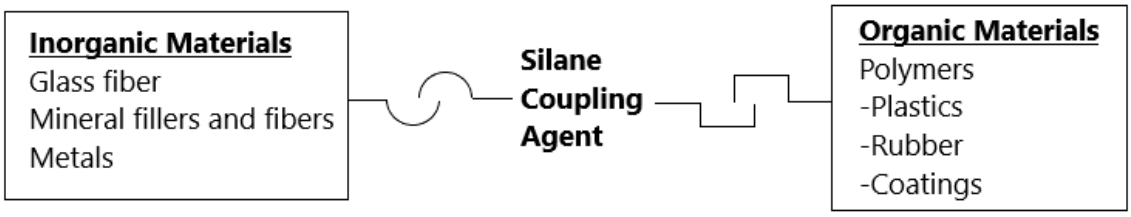

Figure 1.6. Schematic representation of dual reactivity of silane coupling agents [78]

Many literature studies confirm that, silane coupling agents can be applied to the inorganic surfaces in either hydrous or anhydrous dispersing mediums [77]. While some literature studies used hydrous medium for silylation such as water [81] and ethanol-deionised water solution [72,82], others used anhydrous medium such as toluene [58,71,83-85] and acetone [77,86]. It should be noted that, even if an anhydrous solvent is used as the dispersion medium, water may be present as either adsorbed water or may come from the air. The mechanism of interaction of the silanization agent with substrate surface is provided in Figure 1.7 for hydrous media. Initially, the hydrolysis of the inorganic groups of the silane coupling agent occurs to form silanol groups (Si-OH). Subsequently, oligomer formation occurs with the elimination of water. Then, the oligomers create hydrogen bond with the surface -OH groups of the substrate. By the end of the drying process, substrate surface is enriched in silanol groups due to covalently bound silanols. In the case of anhydrous dispersing medium, the covalent binding of silane coupling agent can be achieved in a single as presented in Figure 1.8 [87].

As a result of the silylation process, the amount of silanol groups which is responsible for the hydrophilicity of the material surface is decreased. The decrease in surface hydrophilicity increases the compatibility of the material with the hydrophobic polymers [80].

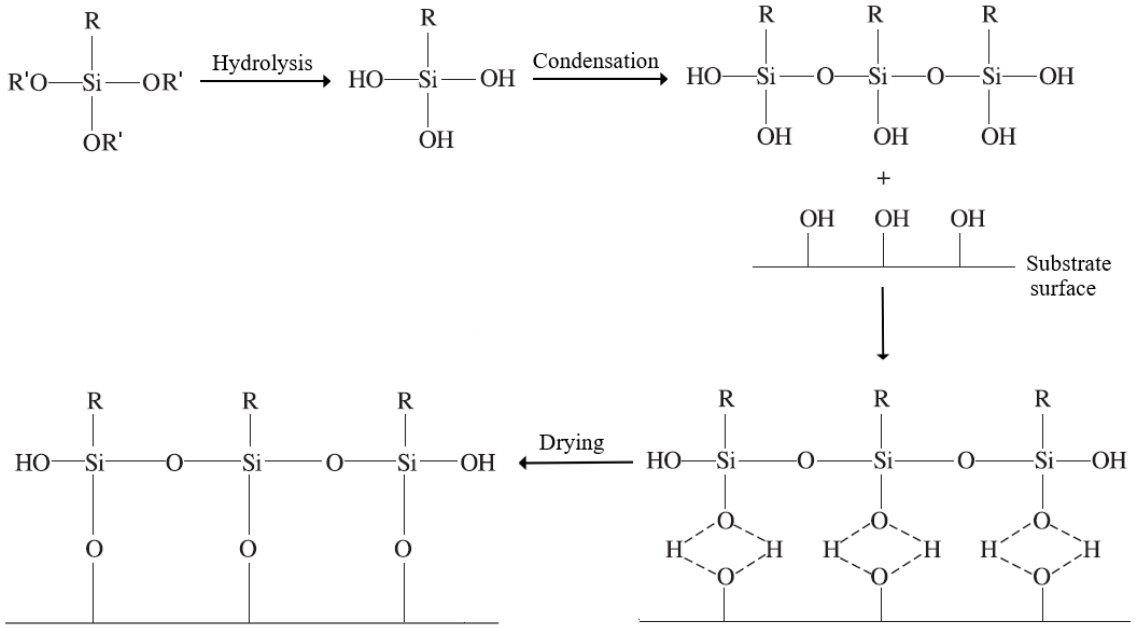

Figure 1.7. The bonding mechanism of silane coupling agent to the substrate surface in hydrous dispersing medium [87]

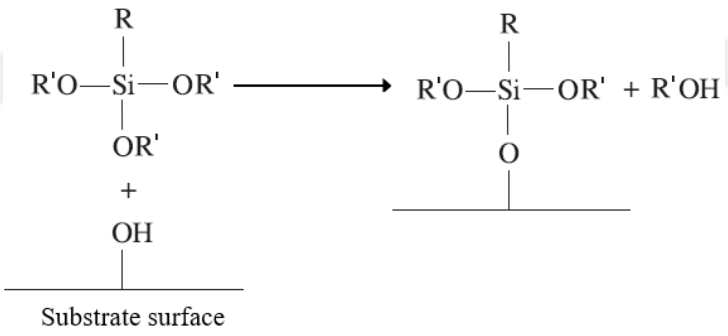

Figure 1.8. The bonding mechanism of silane coupling agent to the substrate surface in anhydrous dispersing medium [87]

1.6. The Effects of Acid Treatment on Sepiolite

Sepiolite can be modified with an acid solution, e.g., HCl [59,88-91], HNO_3 [90,92,93] and H_2SO_4 [56,94] and this process is called as acid treatment. Acid treatment causes several effects on sepiolite. Depending on the acid concentration, the acid treatment of sepiolite leads to removal of the octahedral cations along with some of zeolitic, coordinated and structural water [95]. Sepiolite fibers tend to crystal bundles because of strong linkages and interactions between them (Figure 1.9a). These crystal bundles cause a decrease in the surface area and active sites, which largely limit the

functionality of the mineral. Acid treatment helps to separate the crystal bundles of sepiolite fibers (Figure 1.9b). These effects increase the surface area and porosity of sepiolite as confirmed in many studies [54,89]. Furthermore, the amount of silanol groups on sepiolite surface can be increased by acid treatment due to additional formed edges resulting from broken bonds during the process. The acid treatment has been also used to purify raw sepiolite by dissolving impurities such as carbonates (dolomite, calcite), gypsum etc [50,54,96]. However, the treatment with excess acid will result in a reduction in microporosity, an increase in mesoporosity, and finally amorphous silica formation [56].

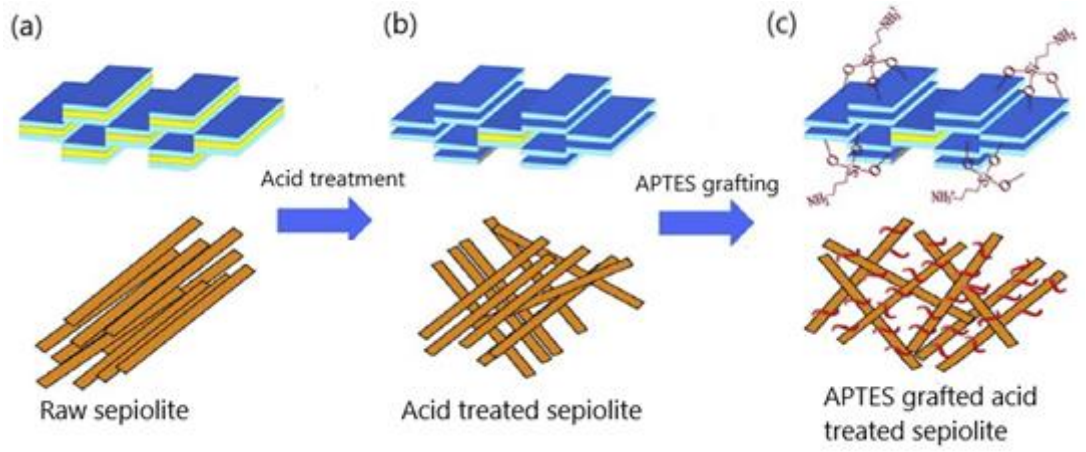

Figure 1.9. Schematic illustrations for (a) raw sepiolite, (b) acid treated sepiolite and (c) (3-aminopropyl)triethoxysilane (APTES) grafted acid treated sepiolite [50].

All these effects contribute to increasing the efficiency of the organic modification when the sepiolite is previously treated with an acid. To separate the crystal bundles of sepiolite, the use of organic modification with the support of the acid treatment is more effective method than the individual use of these methods (Figure 1.9c) [50].

1.7. Methods of Synthesis of Clay-Polymer Composites

The synthesis methods for clay-polymer composites are categorized into three major groups namely, in situ polymerization, solution blending and melt blending, according to the raw materials used and processing methods applied [97].

1.7.1. In-situ polymerization method

In this technique, organoclay is swelled in either liquid or solution of a monomer in order to insert the monomer within the interlayer of clay. Subsequently, the polymerization reaction is started by heating, applying radiation or inserting a suitable initiator into the system. Polymerization generates long polymer chains within the interlayer of the clay. By terminating of the polymerization reaction using a proper catalyst, the clay-polymer composite is obtained (Figure 1.10.) [97-99].

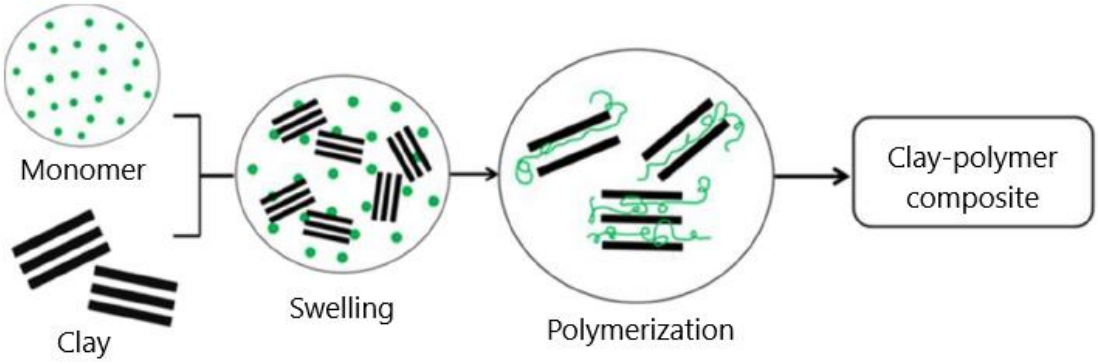

Figure 1.10. In situ polymerization method [97]

1.7.2. Solution blending method

In solution blending technique, the clay is first disaggregated in a solvent or solvent mixture in which the polymer is soluble and the clay is dispersible. The clay-solvent solution is then blended with the polymer to displace the solvent molecules within the interlayer of the clay with the polymer chains. Afterwards, the clay-polymer composite is obtained with evaporation of the solvent. The main challenge of solution blending method is that the selected polymer should be miscible with the selected solvent. Therefore, this method can be useful for only particular clay/polymer/solvent systems. Furthermore, this technique requires a great amount of solvents that are not eco-friendly and bring high production costs (Figure 1.11) [74,97,100].

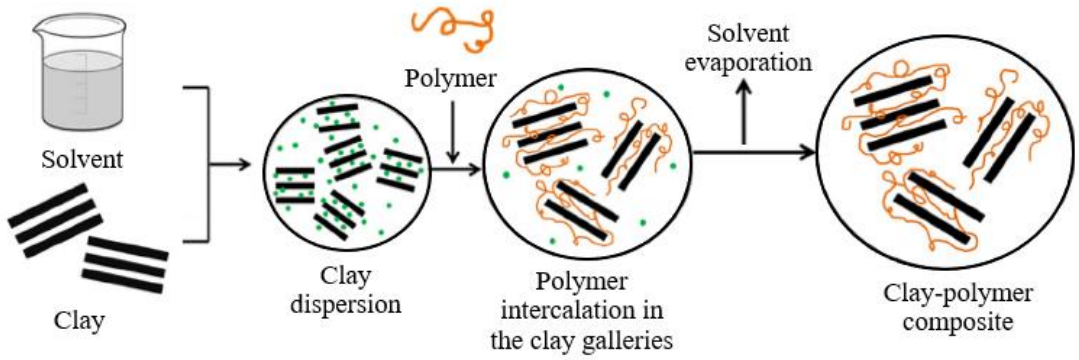

Figure 1.11. Solution blending method [97]

1.7.3. Melt blending method

In melt blending technique, polymer and clay are mechanically mixed at elevated temperature with an extruder or an internal mixer. During the process, the molten polymer enters the voids of the clay. Therefore, this method allows direct compounding of the polymer and clay without need for any solvent. Melt blending has many advantages over solution blending and in situ polymerization methods. Melt blending is environmentally friendly and economically attractive method since no solvent is required for the application. The absence of the need to select a suitable monomer or a compatible solvent makes melt blending more useful and simpler method. It allows the use of polymers that are not applicable for other two synthesis methods (Figure 1.12) [74,97,100].

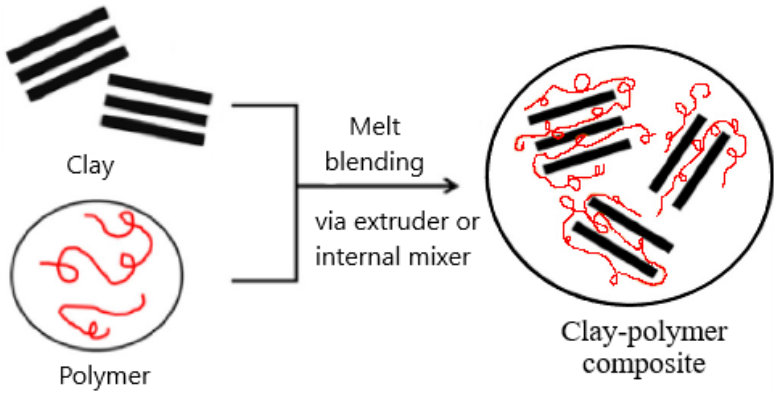

Figure 1.12. Melt blending method [97]

1.8. Polymer Foams

Polymer foams are materials whose skeletal structure consist a great number of cavities surrounded by polymer matrix [100] and they are also called as "cellular polymers", "expanded plastics" etc. The cavities exist in the structure are often referred to as "cells" which give a porous morphology and lightweight to the polymer foams [101].

The characteristic parameters of the porous morphology are the average cell size, and its range in the foam structure, the density of both the cells and the whole bulk foam. The size of a cell can be specified by measuring the diameter of the cell. Cell density refers to the amount of cell per unit foam volume. The density of the foam is found by the ratio of the mass of the foam to its volume. For the foams that have the identical foam density, the size and density of cells are generally inversely proportional parameters [102]. Polymer foams are commonly utilized in broad range of industrial areas including packing, textile, construction, pharmacology, biomedical applications, oil recovery processes, etc. [53,103,104].

1.8.1. Production methods of thermoplastic polymer foams

The synthesis of thermoplastic polymer composite foams is based on the direct use of a foaming agent that gives the cellular morphology to the foam. Two kinds of blowing agents are generally utilized in the foaming processes, namely chemical and physical blowing agents [103]. Chemical foaming agents supply gas molecules (e.g. mostly carbon dioxide or nitrogen) to the material either as a result of a chemical reaction or by decomposition by the effect of temperature [105]. However, the chemical foaming agents are also produced the side-products along with the gas molecules and the removal of these chemical residues necessitates additional purification process. This challenge can be overcome with physical foaming agents whose utilization in the foaming processes does not left chemical side-products in the final foam material [106]. Various organic and inorganic gases have been used as physical foaming agent. Carbon dioxide (CO_2) and nitrogen (N_2) are favorable foaming agent options as these inert gases are nontoxic, non-flammable, low-priced and eco-friendly [103].

In general, the physical foaming of the thermoplastic polymers is accomplished by either batch (discontinuous) foaming that is carried out in a high pressure reactor or

continuous foaming using extrusion and injection molding techniques [103,104]. For all techniques, the fundamental principle of the physical foaming is based on four successive steps, namely, polymer saturation, cell nucleation, cell growth and cell stabilization. Each of these steps is explained as follows:

i. Initially, the polymeric material (either neat polymer or its composites) is saturated (for batch foaming process) or impregnated (for continuous foaming processes) with a foaming agent to form a polymer-gas solution under predetermined saturation conditions.

ii. After sufficient time for the formation of polymer-gas solution, the solubility of the gas in the solution is reduced by creating a sudden thermodynamic instability in the system which results the cell nucleation. Cell nucleation is a process that generates a great number of small gaseous bubbles in polymeric material [105]. The cells can be nucleated either by "homogeneous nucleation" or "heterogeneous nucleation" mechanisms. If the polymeric material has amorphous structure (i.e., its structure does not contain crystal regions) and do not contain any foreign additives in its structure, the cell nucleation occurs randomly and spontaneously. While the already nucleated cells are growing at the same time the new cells continue to nucleate. This nucleation mechanism refers to the homogeneous nucleation represented in Figure 1.13a [102,107]. On the other hand, if the polymer has different bodies in its structure such as crystalline regions and/or foreign additives, the cell nucleation does not happen spontaneously. The foreign bodies in the polymer structure act as nucleation sites that force cell nucleation to occur at the boundary of the additive and the polymer. Since, cell nucleation and growth are supported by the presence of the foreign bodies, the cell growth occurs simultaneously, which promotes smaller cell size and distribution in the final foam material. This nucleation mechanism refers to the heterogeneous nucleation represented in Figure 1.13b [102].

iii. With the decrease in the solubility of the gas in the polymer, the cells continue to grow by diffusion of the dissolved gas molecules from the polymer into the nucleated cells until system reaches equilibrium. While the polymer density decreases during the cell growth, the foam morphology gradually takes form [105,107].

iv. Finally, the obtained cellular morphology is stabilized by cooling of the foamed sample. The cooling process leads to solidification of the final foam by crystallization (for semi-crystalline polymers) or vitrification (for amorphous polymers), which arrests the further expansion of the cells and fixes the final foam morphology [108].

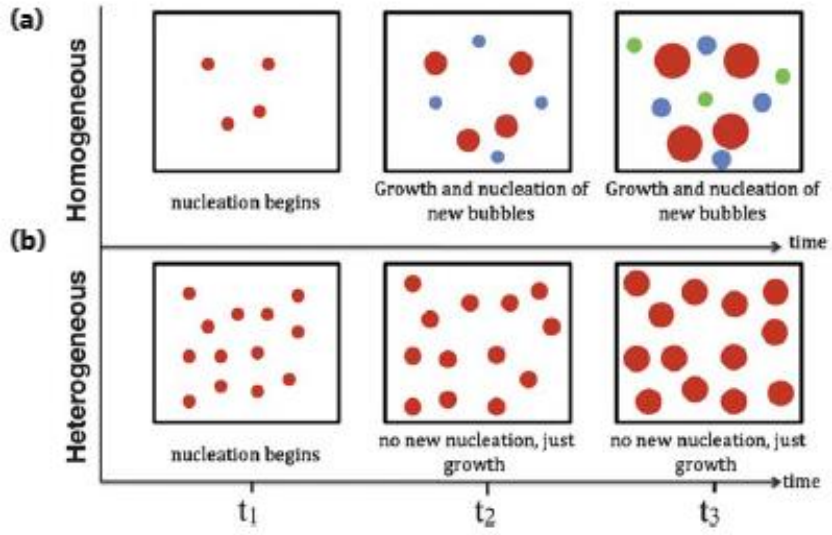

Figure 1.13. Schematics of (a) homogeneous nucleation and (b) heterogeneous nucleation [102].

Batch foaming process is a discontinuous process which is usually carried out in a high pressure reactor (i.e., closed system). In batch foaming, the foaming process can be carried out by two different routes, namely, "pressure induced technique" and "temperature induced technique". In pressure induced technique, the polymeric sample (e.g., neat polymer, polymer composites, copolymer, etc.) is put in a high pressure reactor and saturated with a foaming agent under predetermined saturation conditions about pressure, temperature and time. After enough saturation time, cell nucleation is initiated by suddenly dropping of the reactor pressure to the atmospheric pressure. Subsequently, the foamed sample is taken out of the reactor and cooled to fix the foam structure (Figure 1.14a). In the temperature induced technique, the polymeric sample is saturated with a foaming agent parallel to the former technique but at relatively low saturation temperatures [104]. However, in this technique, the sudden pressure release does not lead to cell nucleation due to the high stiffness of the polymer matrix saturated in low temperatures [103,109]**.** To initiate cell nucleation and growth, the saturated

sample is removed from the reactor and transferred to a hot liquid bath (e.g., oil, water, etc.). The increase in temperature tremendously decreases the solubility the foaming gas in the polymer, which results cell nucleation. Concurrently, the applied temperature leads to soften of the polymer by enhancing the mobility of the polymer chains, which facilitates the growth of the nucleated cells. Finally, the foamed sample is cooled to fix the cellular structure (Figure 1.14b) [110].

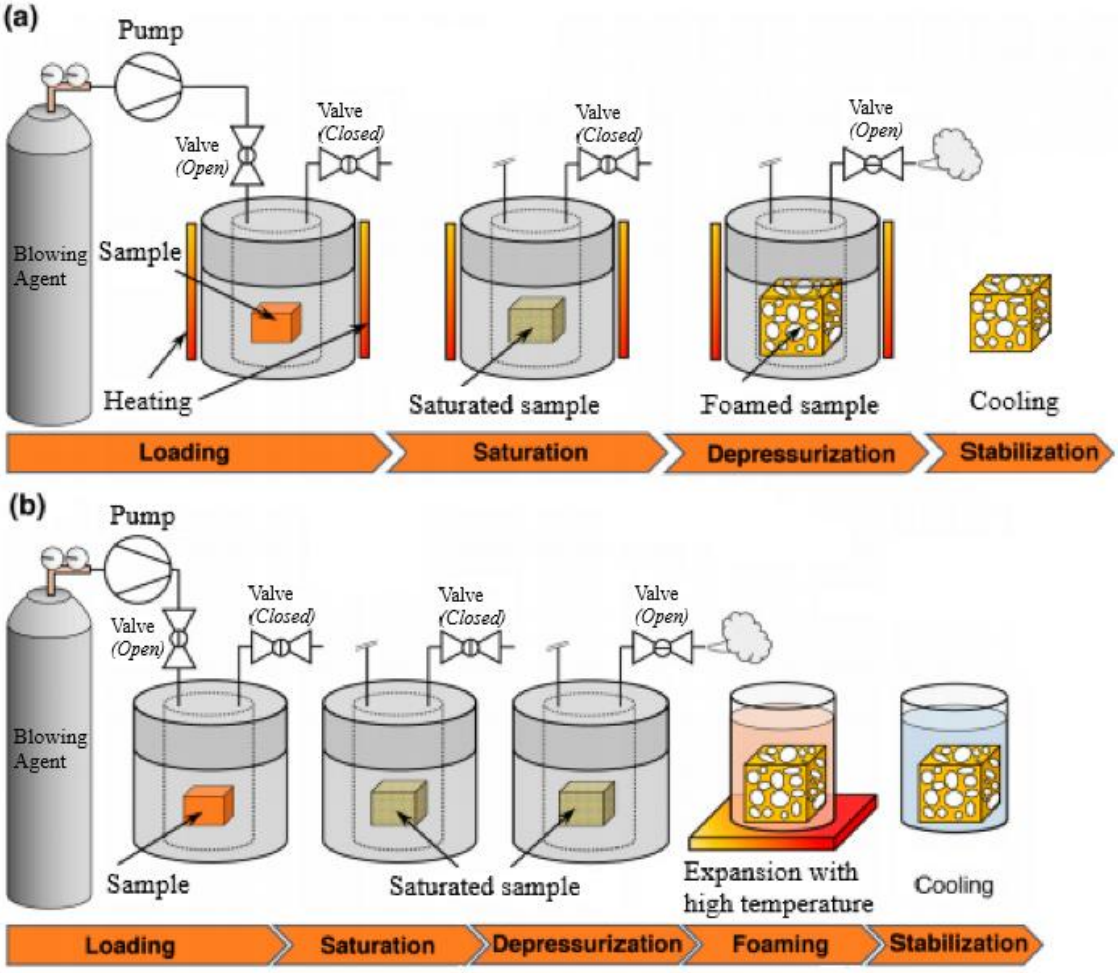

Figure 1.14. Schematics of (a) pressure induced technique and (b) temperature induced technique [110].

Polymer foams can also be produced by continuous process methods, including foam extrusion and injection molding. In the foam extrusion method, the polymer pellets are mixed with a foaming agent under high temperature and pressure. As the polymer-gas solution exits from the die of the extruder, the sudden pressure drop sharply reduces the gas solubility in the polymer, resulting in cell nucleation and growth. Then, the foamed

sample is cooled. The foam production with injection molding is based on a typical injection molding process with an extra foaming agent unit [109,110].

1.8.2. Multifunctional effects of filler on foam morphology

The high porous morphology and lightweight of polymer foams make them efficient oil absorbent materials for use in oil removal applications [111,112]. The porous morphology offers a large surface area and sufficient space for enhanced oil absorption. In the literature, it is possible to find many studies that have been studied on polymer based foams as an oil absorbent material [36,37,112,113]. The characteristic parameters of the porous morphology, namely, average cell size, the density of cells and the foam, and cell size distribution are critical determinants of the oil absorption performance of the polymer foams [112]. Besides good oil uptake performance, a good oil absorbent must have good mechanical properties to withstand marine conditions. However, pure polymer foams generally exhibit inferior mechanical properties due to their porous morphology [102]. The morphology parameters have substantial effect on the mechanical properties of polymer foams. Therefore, the control of the porous morphology parameters has great importance for the design of an optimal foam absorbent product to be used as an efficient oil absorbent material [112].

To control foam morphology and reinforce polymer matrix, the inorganic particles can be introduced to the foam morphology by foaming of the polymer composites called as "polymer composite foams" [100].

The use of inorganic particles within the polymer matrix provides improvement in the mechanical properties of polymer foams and enables to design the morphology and characteristics of the foam [102]. The multifunctional role of the inorganic particles on the polymer foaming process is explained as follows:

- The inorganic particles significantly affect the cell nucleation mechanism, serving as nucleation centers that create locations for cell formation. The nucleation centers restrict cell expansion during the foaming process, which not only reduces cell size but also leads to more homogeneous cell size distribution [104,114]. These centers allow more bubbles to form simultaneously during the foaming process, which explains the reduction in cell size [103]. The foams having smaller cell size exhibit

better mechanical properties than the foams having larger cells. This function of the inorganic particles allows to control the foam morphology and thus mechanical properties of the foams by controlling the foam morphology parameters [102].

- The inorganic particles significantly improves mechanical strength and stability of eventual foam morphology by reinforcing to the polymer matrix without causing a loss of other properties [101,102]. They serve as a protective layer on the cell walls, preventing the rupture of foam morphology under stretching forces [104,114].
- The inorganic particles also affect the foam structure by altering polymer rheological properties. During the expansion of the foam cells, the cell walls become thinner and the neighbour cells get in touch with each other, which decreases the durability of the cell walls. The decrease in the durability increases the coalescences of the neighbour cells, which in turn, increases cell size and decreases the cell density of the foam. Thus, cell coalescence is undesirable, especially for the foaming of the polymers with low melt strength [115]. At this point, the inorganic particles can effectively enhance the melt viscosity of the polymer, which prevents possible cell coalescences at the final stage of cell formation, thereby causing a significant increase in cell density and thus considerable foam expansion [102].
- Furthermore, the surface properties of inorganic particles can be easily modified to increase compatibility with the polymer matrix [102].

The efficiency of the inorganic particles depends on the particle's dimension, shape, aspect ratio, surface chemistry, loading amount of the particles and the degree of compatibility between the particles and the polymer matrix [103]. These parameters provide to control foam morphology and thus mechanical properties. The use of nano-sized inorganic particles is more advantageous over traditional micro-sized ones. Nanoparticles create more potential nucleation centers per unit foam volume at the same particle loading, which in turn promotes to obtain smaller cell size [102,106]. Nanoparticles may be in plate, spherical, or fiber forms. Particles with a spherical shape do not provide sufficient reinforcement than others [102]. Plate shaped nanoparticles may decrease gas diffusion in the matrix phase [100]. The dispersion quality of the particles is important for foam morphology. The well-dispersed particles can improve the nucleation efficiency, when a large quantity of agglomerates is not present in the

matrix phase [116]. Surface chemistry plays an important role in achieving an improved compatibility between the particle and matrix phase, which supports improved particle distribution. With the tuning of the particle loading, it is possible to obtain optimum foam morphology by limiting the amount of the nucleation centers thereby cell expansion capacity [104].

Nanoclays are one of the prefable additives to modify foam structure due to their extremely fine particle size, high surface area and aspect ratio and easily tuneable surface chemistry [102]. To improve the compatibility between the particle and polymer matrix, the organophilic surface properties can be easily attached to the particle surfaces by the surface modification methods such as cation exchange reactions, grafting of silane coupling agents etc. [103].

1.9. The Aim of the Thesis

From past to present, various types of oil have been reaching to the aqueous sources mainly through exploration, production, transportation and consumption related oil spills, natural oil leakages, operational oily waste discharges left by vessels, untreated industrial and urban wastewaters. The presence of oil in water mainly damages marine life, fishing and marine industry, various social and economic activities. Therefore, the spilled oil must be cleaned using a suitable cleaning technique before it is exposed to various weathering processes that make it more tedious to separate the oil from the water.

For this reason, the main purpose of this thesis is to synthesize an environmentally friendly, efficient, durable, and reusable oil absorbent material that can absorb oil from water surfaces and then easily desorb the oil when it is squeezed. As oil absorbent material, a polymer composite foam which is composed of waste LDPE and organically modified sepiolite was synthesized. The synthesized samples were characterized, and their absorption capacities were determined for clean olive oil, waste olive oil, diesel and gasoline. The clean and waste olive oil were used to represent the oil pollutants in urban waste waters, while diesel and gasoline were used to represents the petroleum products related spills. The high porous morphology of foams offers a sufficient space for enhanced oil absorption and their flexible nature allows to easily recover of the absorbed oil. Furthermore, the hydrophobic nature of LDPE matrix brings the

selectively oil absorption quality to the foam. With the use of sepiolite, it is aimed to optimize the foam morphology and improve the mechanical properties of the foamed samples. It is expected that, the use of the synthesized LDPE-sepiolite composite foam as an oil absorbent will not only benefit to the oil remediation in aquatic environment and plastic pollution, but also provide a useful commercial product by utilizing both sepiolite which has significant reserves in Turkey and polyethylene wastes which have considerable portion of the municipal plastic wastes.

2. MATERIAL AND METHOD

2.1. Materials

The materials used in this thesis are as follows:

Waste low density polyethylene (LDPE) pellets were used as the polymer matrix. Raw sepiolite supplied from Dolsan Madencilik in Eskişehir as inorganic filler. Trimethoxy(octadecyl)silane (≥90%), (3-glycidyloxypropyl)trimethoxysilane (≥98%) and (3-aminopropyl)triethoxysilane (≥99%) were supplied from Sigma-Aldrich and used for surface modification of sepiolite (Table 2.1.). Hydrochloric acid (37%, Merck) was used for acid treatment of sepiolite. Toluene (≥99%), acetone (reagent grade) were used as dispersing medium for silylation of sepiolite. Ethanol (reagent grade) was used to wash sepiolite samples after silylation process. Carbon dioxide (CO_2) was used as physical blowing agent in foaming experiments. Extra virgin olive oil was purchased from local suppliers. Gasoline and diesel oils were kindly provided by Asis Otomasyon A.Ş. Waste olive oil was collected from households after cooking.

Table 2.1. Silane coupling agents [117-119]

Name	Chemical structure	Molecular Weight (g/mol)
Trimethoxy(octadecyl)silane	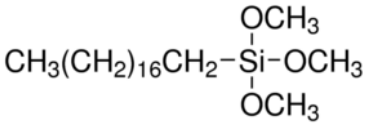	374.67
(3-glycidyloxypropyl)trimethoxysilane	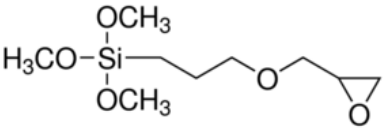	236.34
(3-aminopropyl)triethoxysilane	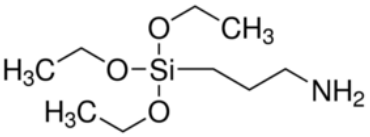	221.37

2.2. Method

2.2.1. Pre-treatment of raw sepiolite

Raw sepiolite was washed with distilled water by mixing in a mechanical stirrer at 400 rpm at ambient temperature for 24 hours (Figure 2.1). After that, the suspension was filtered through a filter paper. The filter cake was dried at 60°C in an oven. The obtained pre-treated sepiolite (SEP) was ground in a mortar and then sieved. Particles sized within the range 75-100 μm were used in further experiments.

Figure 2.1. The pre-treatment of raw sepiolite

2.2.2. Acid treatment of sepiolite

The acid treated sepiolite sample was prepared by mixing the pre-treated sepiolite with 3M hydrochloric acid (HCl) in a mechanical stirrer at 200 rpm, at ambient temperature for 24 hours. Subsequently, the mixture was filtered through a fine filter paper. The sample was washed with water to remove excess HCl and then filtered again. The filter cake was dried at 40°C in an oven. The obtained acid treated sepiolite (ASEP) was ground in a mortar and then sieved to obtain particle size of <100 μm.

2.2.3. Surface modification of both pre-treated and acid-treated sepiolite by different silane coupling agents

A series of organomodified SEP and ASEP samples were prepared for duration of 2 to 48 hours at 25°C, 40°C and 50°C to assess the effect of acid activation, silylation temperature and duration on the extent of organofunctionality of sepiolite. TMODS, GPTMS and APTES were used to modify the surfaces of SEP and ASEP samples. Dispersing mediums were selected considering the solubility of silane coupling agents in solvents. Accordingly, toluene was used for TMODS and acetone was used for both GPTMS and APTES modification reactions.

For each silylation process, 1 ml silane coupling agent was dissolved in 10 ml selected solvent medium for 1 hour. Subsequently, 1 g sepiolite sample (SEP or ASEP) was added to the solution and the mixture was stirred at 120 rpm at different reaction conditions that are given in Table 2.2. At the end of the silylation process, the mixture was filtered, and the filter cake was washed with ethanol for several times to remove excess silane coupling agents. Finally, the sample was dried at 40 °C in an oven. The organo-sepiolite sample to be used as additive in the polymer composites was synthesized on a larger-scale with the same procedure with a reflux apparatus (Figure 2.2.)

Figure 2.2. Large scale silylation process using reflux apparatus

The prepared samples were labelled as "x-y-z-t", where x represents the type of sepiolite used (either SEP or ASEP), y represents the silane coupling agent used (TMODS, GPTMS or APTES), z represents the duration of silylation and t represents the temperature of silylation. The sample designations and their reaction conditions are given in Table 2.2.

Table 2.2. The reaction conditions of the synthesized organomodified sepiolites with the sample designations.

Sample designation	Reaction conditions	Sample designation	Reaction conditions
SEP-TMODS-48-40	For 48h at 40°C	ASEP-TMODS-24-40	For 24h, at 40°C
SEP-TMODS-48-50	For 48h at 50°C	ASEP-TMODS-24-50	For 24h, at 50°C
SEP-GPTMS-4-25	For 4h at 25°C	ASEP-TMODS-48-50	For 48h, at 50°C
SEP-GPTMS-4-40	For 4h at 40°C	ASEP-GPTMS-2-25	For 2h, at 25°C
SEP-GPTMS-4-50	For 4h at 50°C	ASEP-GPTMS-4-25	For 4h, at 25°C
SEP-GPTMS-8-40	For 8h at 40°C	ASEP-GPTMS-4-40	For 4h, at 40°C
SEP-GPTMS-8-50	For 8h at 50°C	ASEP-GPTMS-4-50	For 4h, at 50°C
SEP-APTES-4-25	For 4h at 25°C	ASEP-GPTMS-8-40	For 8h, at 40°C
SEP-APTES-4-40	For 4h at 40°C	ASEP-GPTMS-8-50	For 8h, at 50°C
SEP-APTES-4-50	For 4h at 50°C	ASEP-APTES-4-25	For 4h, at 25°C
SEP-APTES-8-40	For 8h at 40°C	ASEP-APTES-4-40	For 4h, at 40°C
SEP-APTES-8-50	For 8h at 50°C	ASEP-APTES-4-50	For 4h, at 50°C

2.2.4. Determination of oil absorption capacity of each sepiolite sample

The oil absorption capacity of all synthesized sepiolite samples was determined to evaluate the oleophilicity of the material. The ultimate goal was to select the sample with highest oil absorption capacity. The selected sample was then utilized as filler for the clay-polymer composites. For this purpose, 0.1 g sepiolite sample was dispersed in 1 ml pure olive oil in an Eppendorf tube by vortex mixer at 2700 rpm for 5 minutes. Then, the sepiolite-olive oil mixture was centrifugated at 6000 rpm at 10◦C for 15 minutes. After that, the supernatant, i.e. unabsorbed olive oil, was carefully removed from the tube. The tube containing saturated sepiolite was weighed and the weight of olive oil

absorbed by sepiolite sample was determined gravimetrically. The oil absorption capacity of each sample was calculated using the following equation:

$$A = (W_s - W_i)/W_i \quad (2.1)$$

where A is the oil absorption capacity (g oil/g sepiolite), W_i is the initial dry weight of sepiolite sample (g) and W_s is the weight of saturated sepiolite sample (g). The oil absorption capacity of each sample was reported as an average of three experiments.

2.2.5. Production of LDPE-organomodified sepiolite composite pellets by melt blending method

LDPE-organically modified sepiolite composites were produced by melt blending method using the twin screw extruder shown in the Figure 2.3. Prior to extrusion, organically modified sepiolite and waste LDPE pellets were dried in a vacuum oven at 80°C for 24 hours to remove adsorbed water on the samples.

Figure 2.3. Twin screw extruder

The extrusion was performed with a temperature profile of 125°C-130°C-135°C-140°C from feed to die zone with 16.6 cycle/min screw rotating speed. 350 g waste LDPE pellets-organically modified sepiolite mixtures containing 5 wt.%, 10 wt.%, 20 wt.% and 40 wt.% organoclay were prepared and fed to the twin screw extruder, respectively. Afterward, the produced wires were cut in a grinder. The obtained pellets were dried at 70°C in an oven.

The composite samples were labelled as CP-5, CP-10, CP-20 and CP-40 corresponding to 5 wt.%, 10 wt.%, 20 wt.% and 40 wt.% organoclay content, respectively. The composition of each sample was given in Table 2.3.

Table 2.3. Composition of LDPE-organosepiolite composite pellets

Materials	CP-5	CP-10	CP-20	CP-40
LDPE (wt.%)	95	90	80	60
Organosepiolite (wt.%)	5	10	20	40

2.2.6. Preparation of LDPE-organosepiolite composite sheets

The composite pellets were moulded using a hot press machine (Figure 2.4) to obtain circular plates with about 6 cm diameter and 1 mm in thickness. For preparation of each composite sheet, certain amount of composite pellet sample was moulded at a barrel temperature of 120°C and 40 bar for 2 minutes. After moulding, the samples were cooled to room temperature. The produced blank and composite sheets were labelled as BS, CS-5, CS-10, and CS-20 according to their organosepiolite content. The obtained disc shaped sheets were then used as the solid precursor in the foaming experiments.

Figure 2.4. Hot press machine

2.2.7. Production of blank and composite foam absorbents by batch foaming method

Foaming experiments were carried out by using batch foaming method. The composite foams were produced using a pressure reactor (model PARR 4575) equipped with a heater (model PARR 4843) (Figure 2.5). The volume of the pressure reactor is 500 ml and maximum allowable operation temperature and pressure are 300 °C and 553 bar, respectively. Readily prepared blank and composite discs were used as solid precursors for the foaming experiments.

The foaming processes were carried out with pressure induced technique of batch foaming method at three different saturation pressures, while the other process conditions, namely, saturation time, saturation temperature and depressurization rate were kept constant. For each foaming experiments, a solid precursor was placed in the high pressure reactor and saturated with CO_2 for 4 hours at 135 °C at 45 bar, 70 bar or 110 bar. At the end of the period, the sample was cooled to the foaming temperature at 103°C. Subsequently, the sample was foamed by rapidly dropping of the reactor pressure to the atmospheric pressure. Then, the foam was quickly removed from the reactor and cooled to the ambient temperature.

Figure 2.5. The heater and the high pressure reactor

The synthesized foam samples were denoted as in the form of “xF-y”, where “x” indicates high, middle, low saturation pressures which were designated as “H”, “M” and

"L", respectively and "y" refers to organo-sepiolite weight percent content (Table 2.4). All of the further foaming experiments were carried out for 4 hours at 135 °C at 70 bar as optimum process conditions.

Table 2.4. The synthesize conditions for foam samples with their designations

Sample designation	Saturation pressure (bar)	Organosepiolite content (wt.%)
LF-0	45	0
MF-0	70	0
HF-0	110	0
LF-5	45	5
MF-5	70	5
HF-5	110	5
LF-10	45	10
MF-10	70	10
HF-10	110	10
LF-20	45	20
MF-20	70	20
HF-20	110	20

2.2.8. Oil absorption capacity tests of foam absorbents

Oil absorption capacity tests were accomplished in two stages. All synthesized foams were subjected to oil absorption tests in the first stage. Four different types of oil, namely, virgin olive oil, waste olive oil, diesel oil and gasoline, were involved in the experiments. For the determination of oil absorption capacity ($g.g^{-1}$), specimens of app. 1 cm^2 were cut from composite foams and placed in containers filled with 3 ml of oil. The containers were shaken for 30 minutes at 150 rpm. Afterwards, the samples were removed from the containers and waited in a strainer to release excess oil for half a minute. The oil absorption capacity of each sample was calculated gravimetrically. All of the oil absorption capacity tests were performed in triplicates and the average of the test results was used.

The foam sample with the highest absorption capacity was used in further experiments which involved oil removal from simulated sea water. Artificial sea water was prepared according to ASTM D1141-98 [120]. For the oil absorption experiments, four different oil-sea water systems were prepared in 100 ml glass beaker with 5 mm layer of olive oil, waste olive oil, diesel oil or gasoline floating on 50 ml layer of simulated sea water. Then, a pre-weighed foam was placed on floating oil layer. After 30 minutes, the foam saturated with oil was removed from the beaker, left in a strainer for half a minute to drip excess oil and weighed again. The oil absorption capacity of the foam was calculated using Eq 2.1. Oil absorption tests were performed three times for each oil type and average values were recorded.

2.2.9 Reusability of the blank and composite foam absorbents

Reusability of each foam sample was investigated by the successive recovering and reusing of the absorbent foams through three operational cycles. All of the oil absorption experiments were performed for three foam pieces cut from each foam using pure olive oil, waste olive oil, diesel oil and gasoline mediums. In each cycle, the oil absorption capacity of the foam pieces was determined by the method described in Section 2.2.8. At the end of each cycle, the absorbed oil was removed by compression and the foams were weighed again. For each cycle, the average oil absorption capacity of three foam pieces and their standard deviations were calculated.

2.2.10. Characterization of the sepiolite samples

2.2.10.1. X-ray diffraction (XRD) analysis

XRD patterns were obtained with Philips PANalytical, X'PERT PRO instrument operating at 40 kV and using Cu-Kα radiation within 2θ=2-80°.

2.2.10.2. Brunauer-Emmett-Teller (BET) analysis

The BET analysis of the acid treated sepiolite and an acid treated TMODS modified sepiolite were performed to determine the changes in the surface structure and porosity of sepiolite after organic modification process. BET analysis measurements were made by nitrogen adsorption using Micromeritics ASAP 2020.

2.2.10.3. Scanning electron microscope (SEM) analysis

The structure of the selected sepiolite samples were analysed by a scanning electron microscope (FEI Quanta Feg 250).

2.2.10.4. Thermogravimetric analysis (TGA)

Thermogravimetric analysis of the acid treated sepiolite and organo-sepiolite samples were made to quantify the grafted silane coupling agent on the surface of sepiolite using TG/DTA instrument. The samples of 10 mg were heated to 700 °C at a heating rate of 10°C/min under N_2 atmosphere.

2.2.10.5. Fourier transform infrared (FTIR) spectroscopy

FTIR analysis of purified sepiolite, acid treated sepiolite and organo-sepiolite samples was performed to provide an idea of the structure of the samples. The FTIR spectra of the samples were obtained with Perkin-Elmer Spectrum One as an average of 8 scans at 4 cm^{-1} resolution within the spectral range 4000–650 cm^{-1}.

2.2.11. Characterization of the foam absorbents

2.2.11.1. Determination of the apparent density and the volume expansion ratio of the foams

The dimensions of the unfoamed sheets and their foams were measured using Schut electronic outside micrometer to determine the apparent density and the expansion ratio. The density of the unfoamed sheets (ρ_o) and their foams (ρ_f) were calculated as follows,

$$\rho = m/V \tag{2.2}$$

where, ρ refers to the density of the sample, m refers to the mass of the sample and, V refers to the volume of the sample. The unfoamed plates and, their foams were cut in certain dimensions to calculate their volumes [113].

The volume expansion ratio (R_v) of the foams was calculated using the following equation [36].

$$R_v = \rho_o/\rho_f \tag{2.3}$$

2.2.11.2. Scanning electron microscope (SEM) analysis

The morphologies of the selected absorbent foams were analysed by a scanning electron microscope (FEI Quanta Feg 250). The cellular structure of the foams was fixed by freezing with liquid nitrogen to break the samples without damaging the foam morphology.

2.2.11.3. Contact angle measurements

The measurement of contact angles was performed using an apparatus composed of a microscope (Nikon) and a digital camera (D90). The surface characteristic of the foam samples, namely MF-10 and MF-20 was determined by dropping 20 μL of deionized water onto each foam surface at room temperature. The contact angles were then determined using Open Source Image software.

3. RESULT AND DISCUSSION

3.1. Pre-Treatment of Sepiolite Ore

Before starting the acid treatment and surface modification experiments, the raw sepiolite was pre-treated by washing distilled water to obtain reduced and more uniform particle size and, remove its visible impurities [58,84]. The pre-treated sepiolite was designated as “SEP”.

3.2. Acid Treatment of Pre-Treated Sepiolite

Some of the purified sepiolite was treated with HCl solution to enhance the surface area and thereby the surface functionality of raw sepiolite by removing the octahedral cations and some water from the crystal structure, separating sepiolite crystal bundles that significantly limit the surface area.

With the acid treatment of SEP, it was also purposed to improve the efficiency of silylation by increasing the amount of the surface silanol groups that can make covalent bond with silane coupling agents. Marjanović et al. (2011) silylated both purified sepiolite and acid-treated sepiolite with (3-mercaptopropyl)trimethoxysilane. According to the FTIR and TGA analysis results, they showed that the silylation efficiency was significantly increased with acid treatment of sepiolite [58].

Furthermore, sepiolite in raw form may contain different impurities such as carbonate minerals (e.g. dolomite, calcite, magnesite, etc.), quartz and other clay minerals [50,121] depending on the location of the mineral deposit. Suarez et. al (2016) investigated the mineralogical properties of six sepiolite specimens obtained from Polatlı in Turkey. They demonstrated that, all sepiolite specimens contain dolomite as major impurity [122]. With the acid treatment of sepiolite, it was also expected to remove the impurities.

3.3. Organophilic Modification of Sepiolite Samples

Organo-modified samples were prepared from both raw and acid treated sepiolite to demonstrate the effect of the acid treatment on silylation reactions. Due to the fact that,

the effectiveness of the silylation may be affected by the temperature and the duration of the reaction and the silane coupling agents used, the experiments were carried out at different reaction durations and temperatures using three different silane agents, namely, trimethoxy(octadecyl)silane (TMODS), (3-glycidyloxypropyl)trimethoxysilane (GPTMS) and (3-aminopropyl)triethoxysilane (APTES). The reaction conditions were previously given at Table 2.2.

3.4. Oil absorption capacity tests of the sepiolite samples

The oil absorption tests were performed to gain insight about increment in organophilicity of sepiolite after applied acid treatment and silylation processes. The objective of the oil absorption tests was to determine the synthesizing conditions that maximize the oil absorption capacity (g oil/g absorbent) and thus organophilicity of sepiolite. Oil absorption capacity of SEP, ASEP and all organoclay samples were given at Table 3.1.

As expected, the acid treatment process significantly affected the oil absorption capacity of acid treated and non-acid treated samples. The oil absorption capacity of SEP was 1.34 $g.g^{-1}$ and this value was increased to 1.57 $g.g^{-1}$ by applying acid treatment only. Acid treatment of SEP not only provided significant increase in surface area and porosity, but also removed impurities from the mineral. Therefore, the absorption capacity of SEP was improved with increasing its surface area, porosity, and purity.

Another important effect of the acid treatment on the sepiolite structure is that it contributes to the formation of additional silanol groups which are active sites for silane coupling agents. When ASEP that has more active sites than those of SEP was used to synthesis of organo-sepiolite samples, it was possible to cover the surface of the sepiolite with more organic silane agents and thus obtain organoclays with higher organophilic surface properties. Accordingly, all organoclay samples synthesized from ASEP showed visibly improved oil absorption capacity than the samples synthesized from SEP under identical reaction conditions.

Table 3.1. Oil absorption capacity of SEP, ASEP and organomodified samples

Sample designation	Oil absorption capacity ($g.g^{-1}$)	Sample designation	Oil absorption capacity ($g.g^{-1}$)
SEP	1.34±0.01	ASEP	1.57±0.02
SEP-TMODS-48-40	1.03±0.01	ASEP-TMODS-24-40	1.80±0.06
SEP-TMODS-48-50	0.99±0.02	ASEP-TMODS-24-50	1.96±0.05
SEP-GPTMS-4-25	0.96±0.02	ASEP-TMODS-48-50	1.74±0.01
SEP-GPTMS-4-40	1.01±0.02	ASEP-GPTMS-2-25	2.54±0.03
SEP-GPTMS-4-50	0.88±0.02	ASEP-GPTMS-4-25	2.77±0.01
SEP-GPTMS-8-40	0.98±0.01	ASEP-GPTMS-4-40	2.62±0.01
SEP-GPTMS-8-50	0.86±0.03	ASEP-GPTMS-4-50	2.46±0.03
SEP-APTES-4-25	1.36±0.03	ASEP-GPTMS-8-40	2.23±0.03
SEP-APTES-4-40	1.45±0.03	ASEP-GPTMS-8-50	2.17±0.05
SEP-APTES-4-50	1.61±0.03	ASEP-APTES-4-25	2.12±0.03
SEP-APTES-8-40	1.60±0.02	ASEP-APTES-4-40	1.82±0.05
SEP-APTES-8-50	1.65±0.03	ASEP-APTES-4-50	1.58±0.04

The influences of the experimental parameters, namely, temperature and duration of the silylation reaction on absorption capacity of the samples were also investigated by performing a series of the reaction under varying reaction conditions. The effect of the reaction conditions on the oil absorption capacity of the samples was different for each sample. As the reaction temperature was increased at identical reaction duration, the oil absorption capacity of TMODS modified samples showed increasing trend, while that of GPTMS modified samples showed decreasing trend. As reaction duration was extended at identical reaction temperatures, it was observed that, the oil absorption capacity of TMODS modified samples was decreased, while that of GPTMS modified samples were increased. APTES did not show a clear behavior in both conditions. These

different trends in the absorption performances were attributed to the volatility difference of the reaction dispersing solvents. As the dispersing medium, toluene was used in modification reactions with TMODS, while acetone was used in modification reactions with GPTMS and APTES. Due to, acetone is more volatile than toluene, the modification efficiency decreased at higher temperatures.

In literature, the oil absorption capacity of sepiolite was studied. Zadaka-Amir et. al (2013) investigated olive oil absorption capacity of sepiolite, montmorillonite and talc in anhydrous environment. They obtained the olive oil absorption capacity of sepiolite, montmorillonite and talc as 0.36 g/g, 0.16 g/g and 0.19 g/g, respectively [42]. Rajaković-Ognjanović et. al (2007) studied the removal of motor oil mixed in water using sepiolite, bentonite and zeolite. The maximum oil absorption capacities were obtained as about 0.22 g/g, 0.17 g/g and 0.17 g/g for sepiolite, bentonite and zeolite, respectively [123]. As a result of the all oil absorption experiments, the best oil absorption performance was achieved with ASEP-GPTMS-4-25 sample whose each gram can absorb about 2.77 g of olive oil. The obtained oil absorption capacity was significantly superior to that of the literature studies. This two-fold increment in olive oil absorption with respect to that of SEP was achieved by both use of acid treatment process and organic modification under optimum silylation conditions. Therefore, the oil absorption capacity of sepiolite samples greatly depends on acid treatment process and silylation conditions. However, to the best of our knowledge, there is no study on the investigation of oil absorption capacity of both acid treated and silylated sepiolite. In this respect, this gap in the literature was filled by oil absorption capacity experiments using both acid-treated and silylated sepiolite. As a result, ASEP-GPTMS-4-25 was selected as filler phase for the use of the production of the clay-polymer composite materials.

3.5. Characterization of Sepiolite Samples

3.5.1. X-ray diffraction (XRD) analysis

XRD analysis was carried out to investigate the mineral content, and the effect of acid treatment and organic modification on the mineral content and structure. Since the highest organic fraction was obtained with ASEP-TMODS-24-50, the analysis was performed with SEP, ASEP and ASEP-TMODS-24-50. The XRD patterns of SEP,

ASEP and ASEP-TMODS-24-50 were given in Figure 3.1.

The XRD pattern of SEP showed strong characteristic peak at 2θ=7.3° and some weak characteristic peaks. Owing to the major impurity of dolomite in SEP, the strong peaks at 2θ=31° and 2θ=41.2° were also observed in the XRD pattern of SEP [124,125]. The XRD pattern of ASEP showed that the characteristic sepiolite and dolomite peaks were dissappeared by acid attack. From the XRD pattern, it can be said that, the crystal structure of sepiolite was seriously affected by acid treatment and turned into an amorphous structure [126]. The formation of covalent bonds between the silane coupling agent and sepiolite surface leads to some structural changes, resulting the change in the peak intensities of the XRD pattern. A comparison of the XRD patterns of ASEP and TMODS modified ASEP proved the modification of ASEP by TMODS by the presence of the peak at 2θ=21.7° [84].

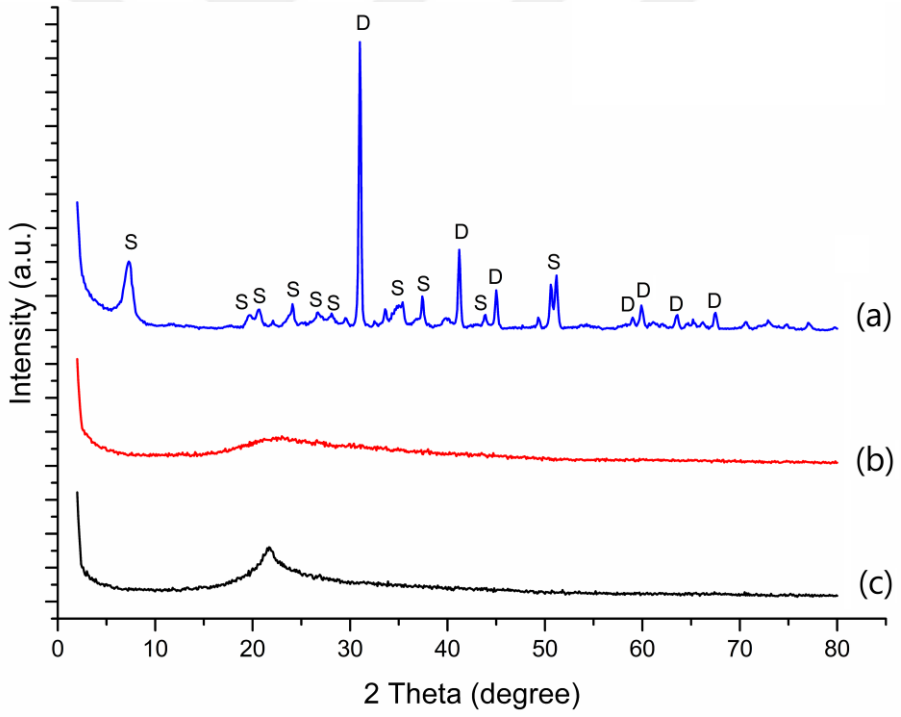

Figure 3.1. XRD patterns of (a) SEP, (b) ASEP and (c) ASEP-TMODS-24-50 (S:Sepiolite and D:Dolomite)

3.5.2. Brunauer-Emmett-Teller (BET) analysis

BET is most common analysis method to measure the specific surface area and porosity of the solid materials. Since the highest organic fraction was obtained with ASEP-

TMODS-24-50, the analysis was carried out for the SEP, ASEP and ASEP-TMODS-24-50 samples given in Table 3.2.

Table 3.2. The BET surface area and pore volume of SEP, ASEP and ASEP-TMODS-24-50

Sample designation	Surface area ($m^2.g^{-1}$)	Pore volume ($cm^3.g^{-1}$)
SEP	31.59	0.17
ASEP	52.05	0.25
ASEP-TMODS-24-50	2.94	0.05

BET surface area and pore volume of SEP sample were measured as 31.59 $m^2.g^{-1}$ and 0.17 $cm^3.g^{-1}$, respectively. After acid treatment, it was observed that the BET surface area and pore volume of the mineral (i.e. ASEP) increased to 52.05 $m^2.g^{-1}$ and 0.25 $cm^3.g^{-1}$, respectively. As mentioned before, with acid treatment of natural sepiolite, Mg^{2+} cations in the octahedral sheets and a part of water can be removed from the sepiolite structure. Also, sepiolite crystal fibres that cause a significant reduction in the specific surface area of the mineral unbundle with the help of acid treatment. All these led to increase surface area and porosity of sepiolite. There are many studies in the literature confirming the increase in the surface area and pore volume of sepiolite with acid treatment. Myriam et al. (1998), reported that, the surface area of natural sepiolite (supplied from Spain) enhanced from 213 m^2g^{-1} to 293 m^2g^{-1} with acid treatment using HCl [89]. More recently, Zhou et al. (2018) also reported improvement in the surface area of sepiolite (supplied from China) from 33 m^2g^{-1} to 198 m^2g^{-1} with acid treatment using HCl [54].

BET surface area and pore volume of ASEP-TMODS-24-50 were recorded as 2.94 $m^2.g^{-1}$ and 0.05 $cm^3.g^{-1}$, respectively. The significant decrease in surface area and pore volume confirm the successful organic modification of ASEP surface by blocking of its channels by the silane coupling agent.

3.5.3 Scanning electron microscope (SEM) analysis

SEM analysis of sepiolite samples was performed to visualize the effect of acid treatment and organic modification on the mineral structure. SEM micrographs of SEP, ASEP and ASEP-TMODS-24-50 were presented in Figure 3.2a-f.

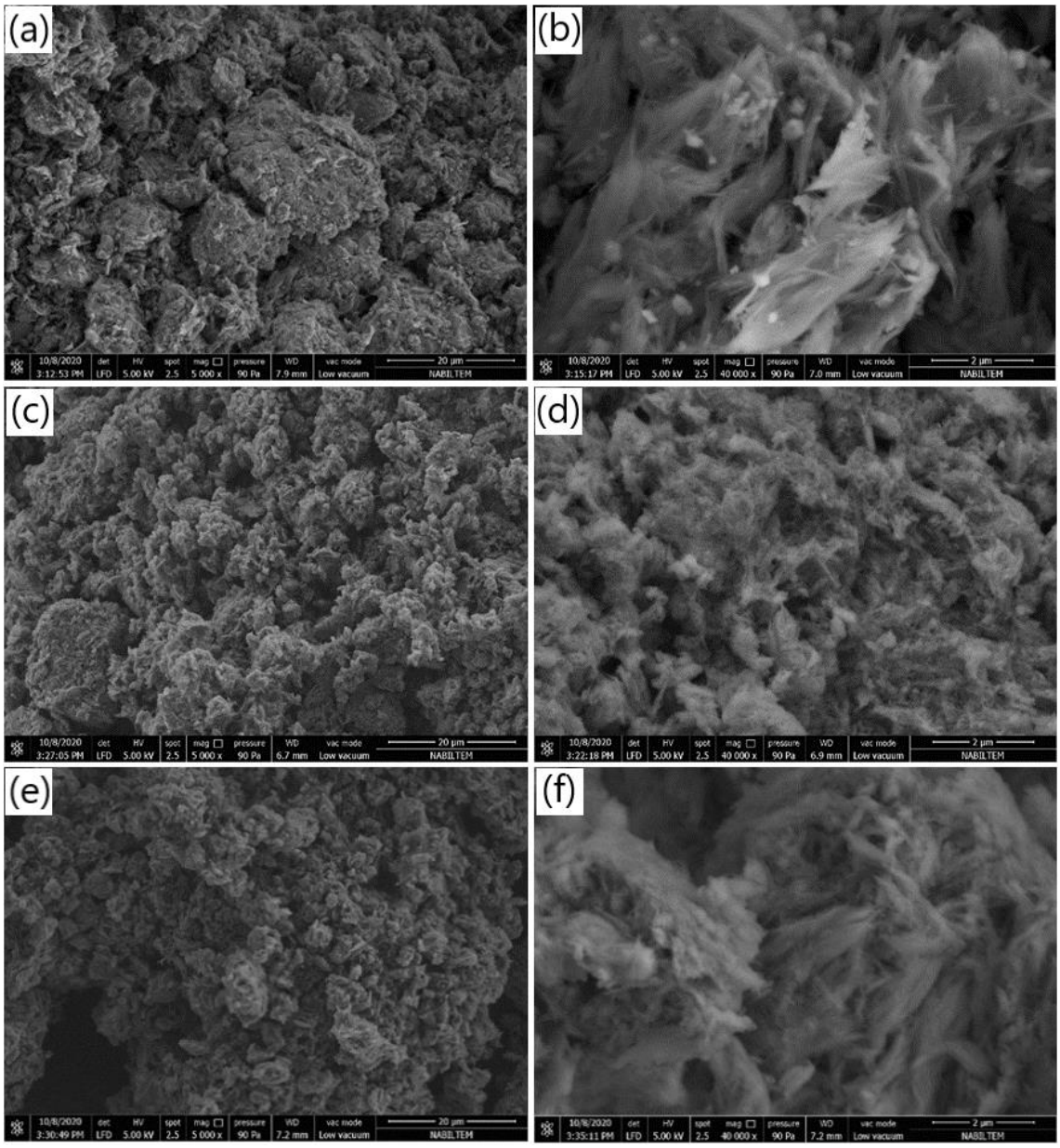

Figure 3.2. SEM micrographs of (a) SEP under the magnification of 5000×, (b) SEP under the magnification of 40000×, (c) ASEP under the magnification of 5000×, (d) ASEP under the magnification of 40000 × , (e) ASEP-TMODS-24-50 under the magnification of 5000×, (f) ASEP-TMODS-24-50 under the magnification of 40000×.

As clearly seen in Figure 3.2a, SEP was in the form of large fiber agglomerates. The characteristic fibrous structure of SEP was more obviously observed in Figure 3.2b. As expected, the fibers were in the form of crystal bundles due to strong interactions between them. These crystal bundles cause a significant decrease in the surface area and active sites, which largely limit the functionality of the mineral [54]. In addition to the

fiber bundles, some spherical materials attributed to impurities were also observed from the SEM micrograph of SEP sample. As clearly seen from Figure 3.2c., the degree of agglomeration was decreased in ASEP compared to SEP. In Figure 3.2d, it was observed that, the mineral lost its fibrous morphology to some extent and the fiber lengths were decreased compared to SEP [54]. Also, the impurities seen in SEP sample were disappeared in ASEP sample due to purification effect of acid treatment. SEM images of ASEP-TMODS-24-50 sample were given in Figure 3.2e-f. From the images, it can be said that, the silylation process did not alter the structure of ASEP, significantly.

3.5.4. Thermogravimetric analysis (TGA)

TGA is one of the thermal analysis techniques that based on measuring the change in the mass of the material as a function of temperature or time [127]. TGA was used to determine the percentage mass of the silane coupling agents loaded on the sepiolite surface after organic modification. DTG curves were used to clearly identify the mass loss steps of the sepiolite samples.

Sepiolite has three types of water, namely, hydroscopic, zeolitic and coordinated water, and also hydroxyl groups in its structure [56]. These water molecules and hydroxyl groups are linked to the sepiolite structure at different strengths [83]. Therefore, the TGA curve of the pure sepiolite exhibits four discrete thermal decomposition steps owing to the gradual removal of these waters from the crystal structure during heating [55,71]. Theoretically, the successive reactions that occur during the thermal decomposition of pure sepiolite are as follows [55]:

$$Si_{12}Mg_8O_{30}(OH)_4(OH_2)_4.8H_2O \rightarrow Si_{12}Mg_8O_{30}(OH)_4(OH_2)_4 + 8H_2O \quad (3.1)$$

$$Si_{12}Mg_8O_{30}(OH)_4(OH_2)_4 \rightarrow Si_{12}Mg_8O_{30}(OH)_4(OH_2)_2 + 2H_2O \quad (3.2)$$

$$Si_{12}Mg_8O_{30}(OH)_4(OH_2)_2 \rightarrow Si_{12}Mg_8O_{30}(OH)_4 + 2H_2O \quad (3.3)$$

$$Si_{12}Mg_8O_{30}(OH)_4 \rightarrow 8MgSiO_3 + SiO_2 + 2H_2O \quad (3.4)$$

If the sepiolite do not contain any impurity, the theoretical percentages of the successive water losses should be 11.11%, 2.78% 2.78% and 2.78% respectively [55]. The initial mass loss occurs due to the removal of the hydroscopic water on the external mineral surface besides the zeolitic water in the structural tunnels and channels of sepiolite (Eq.

3.1). Then, the coordination water gradually removes from the mineral (Eq. 3.2 and Eq. 3.3). At the end of the dehydration steps, sepiolite anhydrite ($Si_{12}Mg_8O_{30}(OH)_4$) was produced as a result of the irreversible loss of all coordinated water [71]. After dehydration steps, the dehydroxylation of the sepiolite anhydride begins, which results the production of enstatite ($MgSiO_3$) and silica (SiO_2) by removing the hydroxyl groups in the structure as structural water (Eq. 3.4) [55]. If the mineral dolomite contains impurities, it also decomposes. Tabak et. al (2009) analyzed Eskişehir sepiolite with TGA. They reported that, the removal of the hydroscopic water on the outer mineral surface was occurred up to 105 °C with a 1.92% mass loss and the zeolitic water was removed in the temperature ranges of 180-232°C with a 0.60% mass loss. Coordination water was removed from the sepiolite with a 1.79% mass loss in the temperature range of 232-326°C. Finally, the structural water was removed and dolomite was decomposed with a mass loss of 13.21% in the temperature range of 580-823°C [124].

TGA and DTG curves of ASEP and selected organo-sepiolite samples were shown in the Figure 3.3a-f. The samples with the highest oil absorption capacity were selected for thermal analysis so as to discuss the possible relationship between the level organic loading and oil absorption. As seen in Figure 3.3a, ASEP exhibited three completed and one uncompleted mass loss steps up to 700°C accounting for 16.4% mass loss in total. The mass loss percentages of ASEP were recorded in the order of 2.1%, 0.8%, 2.7% and 10.8% in the temperature ranges of 35-147°C, 147-315°C, 315°C-545°C and 545-700°C respectively. The first three mass losses were respectively attributed to the removal of hydroscopic, zeolitic and coordinated water from the mineral. The fourth mass loss step was not completed at 700°C with a 10.8% mass loss. This mass loss was attributed to both the removal of structural water and the residual dolomite decomposed by acid treatment owing to the insufficient washing of the mineral. In the TGA of ASEP, the mass losses only occurred due to the removal of water molecules and the residual dolomite.

Comparison of the TGA of organomodified sepiolite samples (Fig. 3.3b-f) with that of ASEP provided a solid proof of the presence of silane grafting upon ASEP surface. In the case of organically modified ASEP samples, the mass loss occurred due to both of the removal of water and the thermal degradation of the silane coupling agents grafted on the surface of sepiolite [55].

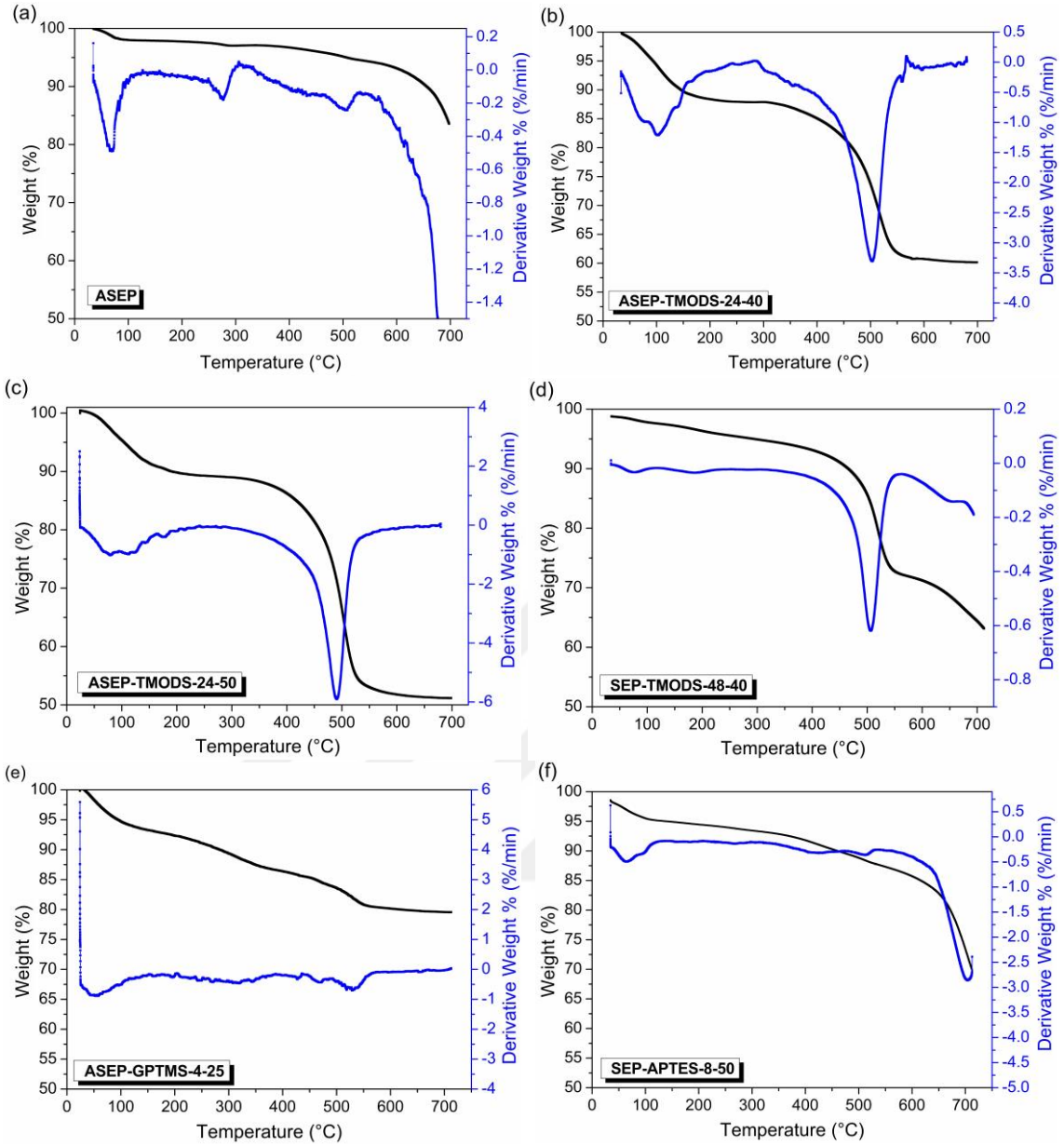

Figure 3.3. TGA and DTG curves of (a) ASEP, (b) ASEP-TMODS-24-40, (c) ASEP-TMODS-24-50, (d) SEP-TMODS-48-40, (e) ASEP-GPTMS-4-25 and (f) SEP-APTES-8-50

It was observed that organomodification process significantly altered the path of thermal degradation steps of sepiolite due to the incorporation of the organic silane agents into the mineral structure. The total mass loss was obtained as 40%, 47%, 36%, 20% and 30% for ASEP-TMODS-24-40, ASEP-TMODS-24-50, SEP-TMODS-48-40, ASEP-GPTMS-4-25 and SEP-APTES-8-50 respectively. The first decomposition steps were attributed to the removal of hydroscopic and zeolitic water corresponding to 12%,

12%, 4%, 7% and 5% mass losses for the same five samples, respectively. The completion temperature of the removal of these waters was detected about 200°C for ASEP-TMODS-24-40, ASEP-TMODS-24-50 and SEP-TMODS-48-40, about 150°C for ASEP-GPTMS-4-25 and about 130°C for SEP-APTES-8-50. According to the literature studies, the mass loss in the temperature range about 200°C-600°C was attributed to the decomposition of silane coupling agents [55,71]. At nearly the same temperature range, TMODS decomposed in one step, while GPTMS and APTES displayed a two-step decomposition profile. The mass loss owing to decomposition of the organic matters were approximately obtained as 28%, 35%, 23%, 13% and 7% for ASEP-TMODS-24-40, ASEP-TMODS-24-50, SEP-TMODS-48-40, ASEP-GPTMS-4-25 and SEP-APTES-8-50 respectively. For the organomodified SEP samples, namely SEP-TMODS-48-40 and SEP-APTES-8-50, after the decomposition of the organic matter, an additional incomplete mass loss step that started between 500°C-550°C was observed (Figures 3.3d and f). This mass loss step was attributed to the decomposition of the dolomite impurity present in the mineral [128]. On the other hand, no further mass loss step was observed after the decomposition of the organic matter for the organomodified ASEP samples. The reason of this, the dolomite impurity was eliminated by acid treatment and the residual dolomite present in ASEP due to insufficient washing was removed along with the silylation dispersing solvent and washing after silylation. DTG curves also confirms the grafting of silane coupling agents on sepiolite. All DTG peaks of in organomodified samples were distinctly appeared near 500°C which was the sign of successfully grafting of the silane agents onto the sepiolite surface. Raji et. al (2018) and Tartaglione et. al (2008) modified natural sepiolite with APTES and they obtained 3.87 wt.% and 4.5 wt.% organic fraction, respectively [55,71].

It should be noted that, the mass percentage of silane molecules in the mineral is directly related to the molecular weight of the silane, since the molecular weights of the three silanes are different from each other. The molecular weight of TMODS, GPTMS and APTES are 374.67 g/mol, 236.34 g/mol and 221.37 g/mol, respectively [117-119]. When the mass percentages of the silanes loaded onto sepiolite were compared, it was seen that these values were directly proportional to the molecular weight of the silanes. Although the highest mass percentage of loaded silane was achieved with TMODS,

most of this mass came from the long hydrocarbon chain of TMODS. Therefore, it is possible to claim that, on molar basis less number of moles of TMODS was loaded upon sepiolite surface with respect to other silanes. The fact that the oil absorption capacity of the samples is not directly proportional to the organic mass percentage of the samples supports this idea. Therefore, the relationship between the organic loading level and oil absorption capacity was discussed. Oil absorption capacity of SEP increased from 1.36 g/g to 1.57 g/g with only acid treatment process. SEP-TMODS-48-40 showed lower oil absorption performance even than SEP despite its high organic content. The reason may be that TMODS's long hydrocarbon chains took up too much space on the SEP surface and pores, resulting in reduced oil absorption performance of the clay. On the other hand, both TMODS modified ASEP samples showed higher absorption capacity and organic loading level than TMODS modified SEP sample due to improved BET surface area and pore volume of the mineral. When ASEP-TMODS-24-40 and ASEP-TMODS-24-50 were compared, it was observed that as the silylation temperature increased, more TMODS was loaded into ASEP and the oil absorption capacity of the mineral increased in parallel. Despite the organic fraction of ASEP-GPTMS-4-25 was low compared to TMODS modified samples, ASEP-GPTMS-4-25 exhibited the highest oil absorption performance. This may be related to the different chemical structure of the silanes.

3.5.5. Fourier-transform infrared (FTIR) spectroscopy

Silane coupling agents can be chemically bonded or adsorbed to the surface of sepiolite, as well as coat on the surface as an oligomer film. While, the coupling agents that coat on or adsorb to the sepiolite surface do not have an impact on FTIR spectra, the coupling agents that chemically bond to the surface of sepiolite effect on FTIR spectra [129]. With the FTIR analysis, it was aimed to show the effect of acid treatment on the sepiolite and confirm the grafting of silane coupling agents onto the surface of sepiolite.

The FTIR spectra of SEP, ASEP, SEP-TMODS-48-40, ASEP-GPTMS-4-25 and SEP-APTES-8-50 were recorded between 4000 and 650 cm^{-1} wave numbers given in Figure 3.4. The FTIR spectrum of SEP showed several characteristic absorption peaks due to the IR vibrations of various types of water existing in the structure of sepiolite, the bonds constituent its lattice and impurities in the mineral (Figure 3.4a). The 4000-3000 cm^{-1} wavelength range corresponds to the stretching vibrations of various types of OH

groups [130]. The slight peaks appeared at 3690 cm^{-1} and 3623 cm^{-1} were attributed to O-H stretching vibrations attached to Mg in octahedral sheets [71,131-133]. The peak at 3556 cm^{-1} was assigned to O-H stretching vibration of coordinated (bound) water [71,92,124,131,134]. The peak appeared at 1662 cm^{-1} was attributed to the O-H bending vibration of zeolitic water [92,124,130]. The peak at 1450 cm^{-1} indicates asymmetric CO_3^{2-}stretching vibrations [89,122,124,130,134], while the peaks at 882 cm^{-1} and 729 cm^{-1} indicate the asymmetric and symmetric bending vibrations of CO_3^{2-}, respectively. These peaks reflect the presence of carbonate minerals within the sepiolite sample used [61,122,125]. The bands located at 1210, 1080 (shoulder), 1006 and 977 cm^{-1} indicate the characteristic lattice bands of sepiolite and were assigned to Si-O stretching vibrations in the tetrahedral sheets [71,83,132,135]. The peaks appeared at 786 and 688 cm^{-1} were attributed to the bending vibration of Mg-OH [125,131].

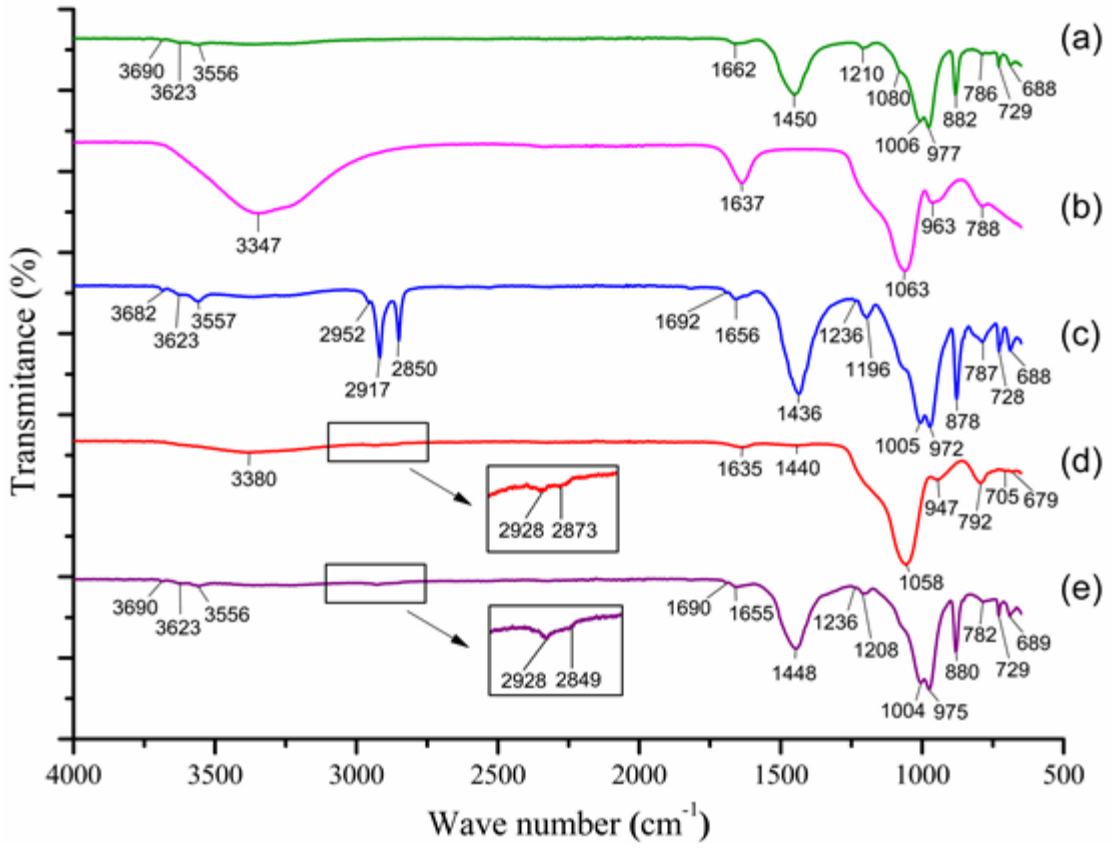

Figure 3.4. The FTIR spectra of (a) SEP, (b) ASEP, (c) SEP-TMODS-48-40, (d) ASEP-GPTMS-4-25 and (e) SEP-APTES-8-50

As seen in Figure 3.4b, the FTIR spectrum of SEP significantly changed with the acid treatment process. In the FTIR spectrum of ASEP, the new broad peak centred at 3347

cm^{-1} may be attributed to the vibration of OH groups, which may indicate the increase in silanol groups (Si-OH) on the mineral surface. The peaks at 1440, 882 and 729 cm^{-1} reflecting the presence of the carbonate minerals that appeared in SEP and disappeared in ASEP due to the purification effect of the acid treatment. Due to the characteristic lattice peaks between 1210 and 977 cm^{-1} is much sensitive to acid treatment, this region of the ASEP's spectrum significantly changed [135]. Also, the peaks related to the bending vibrations of Mg-OH at 786 and 688 cm^{-1} altered as a result of the dissolution of the octahedral layers of the mineral by acid attack [89,92]. These alterations in FTIR spectrum of ASEP clearly showed that, the acid treatment considerably changed the lattice structure of sepiolite, which further verified XRD results (Fig. 3.1).

After organic modification process, the FTIR spectra of organosepiolite samples showed a similar path with the sepiolite sample (SEP or ASEP) from which they were synthesized, except from the new peaks from grafted silane coupling agents. This indicates that, the organic modification process does not damage the lattice structure of sepiolite like the acid treatment process. As seen in Figure 3.4c, the FTIR spectrum of SEP-TMODS-48-40 exhibited two deep bands at 2917 and 2850 cm^{-1}, respectively assigned to the stretching vibrations of C-H bonds of methoxy groups ($O-CH_3$) and the methylene groups ($-CH_2$) present in the long hydrocarbon chain bonded to the Si atom of TMODS [58]. In Figure 3.4d and 3.4e, the similar peaks were also observed at 2928 and 2873 cm^{-1} for ASEP-GPTMS-4-25 and, 2928 and 2849 cm^{-1} for SEP-APTES-8-50 owing to the presence of the methoxy and the methylene groups in their structure but at lower intensity compared to that of SEP-TMODS-48-40. The existence of these peaks confirmed a successful modification of surface of sepiolite with all the three silane coupling agents. Moreover, the peak observed in the spectrum of ASEP at 3347 cm^{-1} related to surface -OH groups, was suppressed and shifted towards lower wave numbers for ASEP-GPTMS-4-25, which also proved the grafting of GPTMS upon ASEP via surface -OH groups.

The FTIR results showed that, the FTIR spectrum of SEP was changed by treatment with the acid and/or the silane coupling agents. The characteristic peaks come from the silane coupling agents were observed the spectrum of each organomodified sepiolite samples. These peaks clearly showed that, TMODS, GPTMS and APTES was successfully grafted onto the sepiolite.

3.6. Production Steps of LDPE-Organosepiolite Composite Foams

3.6.1. Production of LDPE-Organosepiolite Composite materials

Thermoplastic polymer composite foams are generally produced via two stages. Firstly, the polymer composite is produced and then the composite material is used as a solid precursor for the foaming process [100]. To obtain solid precursors for foam production, composite pellets were produced first and then they were formed into sheets. As filler phase, ASEP-GPTMS-4-25 organosepiolite sample was used, while LDPE was used as polymer matrix in the production of the composite pellets. The composite pellets were produced by melt blending technique using a twin screw extruder. Four different pellets containing 5%, 10%, 20% and 40% organosepiolite by weight were prepared and named as CP-5, CP-10, CP-20 and CP-40 respectively (Figure 3.5). While the CP-40 pellet was eliminated due to its insufficient durability and, it was decided to continue with CP-5, CP-10 and CP-20 pellets in further experiments.

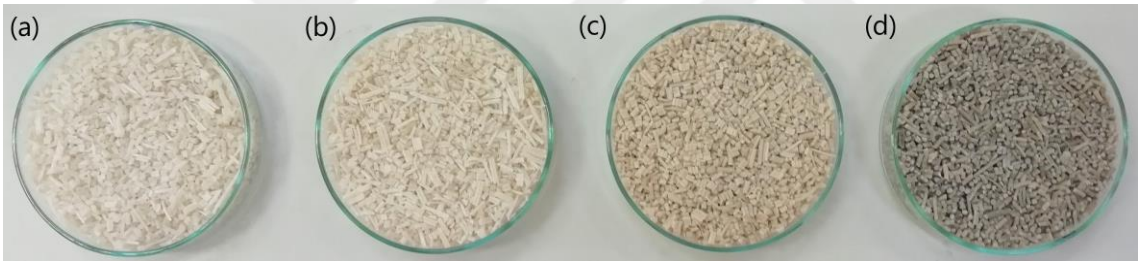

Figure 3.5. The images of (a) CP-5, (b) CP-10, (c) CP-20 and (d) CP-40 composite pellets

Both waste LDPE pellets and synthesized composite pellets were transformed into sheets using a hot press machine for use as solid precursor in the foam production. The blank and composite sheets are presented in Figure 3.6. In foaming experiments, the geometry of the polymeric solid precursors is an important point in the foaming experiments. The samples are generally prepared in the form of disc-shaped, square-shaped or rectangular-shaped and their thickness should be not more than 3 mm not to inhibit the diffusivity of the foaming gas [104,107]. For this reason, the sheets were prepared in 1 mm thickness and disc-shaped form. The sheets prepared from waste LDPE, CP-5, CP-10, and CP-20 pellets were labelled as BS, CS-5, CS-10, and CS-20, respectively.

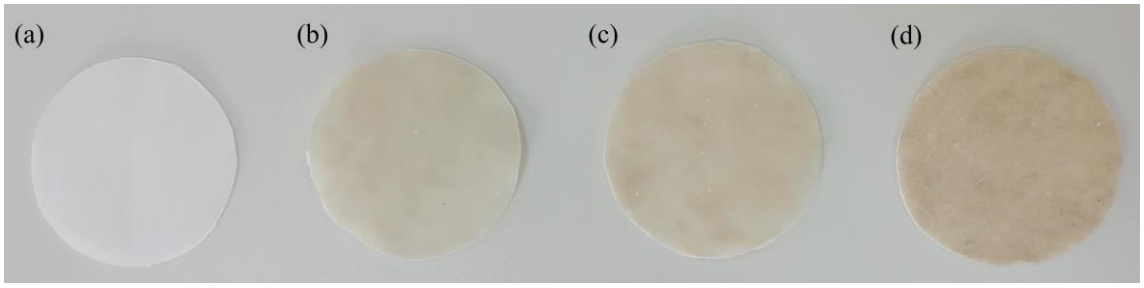

Figure 3.6. The images of (a) BS (b) CS-5, (c) CS-10 and (d) CS-20 sheets

3.6.2. The applied strategy for foam synthesis and determination of the synthesis conditions

The characteristics of a foam, i.e. cellular morphology and volume expansion ratio are both related to the foam synthesis conditions and, the properties of the materials from which it is made. The most important synthesis conditions are the temperatures of saturation and foaming, pressure and duration of saturation, and depressurization rate.

The obtained LDPE and the composite sheets were used as solid precursor in the foaming experiments. The foaming of the sheets was carried out by the pressure induced technique of the batch foaming method using a high pressure reactor. For the foaming process, the solid precursor was put into the reactor. After the reactor was loaded with physical foaming agent (CO_2), the reactor was heated to the saturation temperature of 135 °C. This saturation temperature was chosen to ensure that the crystalline regions of LDPE matrix melts completely. To investigate the effect of saturation pressure on the foaming processes, the samples were saturated at three different saturation pressures, 45, 70 and 110 bar. The materials were saturated with CO_2 for 4 hours to guarantee completed saturation. After the saturation of the material was completed, the reactor was cooled to the foaming temperature. For determination of the optimum foaming temperature, several foaming experiments were performed at different foaming temperatures. LDPE matrix maintains its durability under the melting temperature. When LDPE is brought to its melting temperature about 110 °C [136], its melting strength begins to decrease. The highest expansion capacity was reached for all foams at the foaming temperature of 103 °C for our pressure reactor. When the materials were attempted to be foamed slightly below 103 °C, the matrix hardly expanded due to the existence of the crystalline regions that may supress the expansion of the matrix [36].

When the foaming temperature was applied above 103◦C, it was observed that the material came out of the reactor as a melt due to the melt strength of the matrix was significantly decreased. After the material was cooled to the foaming temperature, the foaming was induced by rapid pressure drop. After that, the foamed material was quickly taken out from the reactor and cooled to stabilize its cellular morphology.

Also, the addition of the foreign materials into the polymer matrix allow to design the cellular morphology, helps to improve mechanical strength by reinforcing to the matrix and enhance the durability of the cell walls by increasing melt strength. If the polymeric material does not contain any foreign bodies, the cell nucleation occurs randomly and spontaneously. [102,107]. On the other hand, if the polymer matrix has different bodies, these materials act as nucleation agents that force cell nucleation to occur at the boundary of the additive and the matrix. Therefore, cell nucleation and growth can be supported by the presence of foreign bodies, which improves the final cellular morphology [102]. In this regard, it is possible to find many studies on the use of inorganic nanoparticles as nucleating agents in the literature [73,106,114-116]. Sepiolite is a proper inorganic additive whose particles have nano-sized dimensions, fiber shape, high aspect ratio and surface area [73]. The foams produced at 70 bar (saturation pressure) with different organosepiolite content were presented in Figure 3.7.

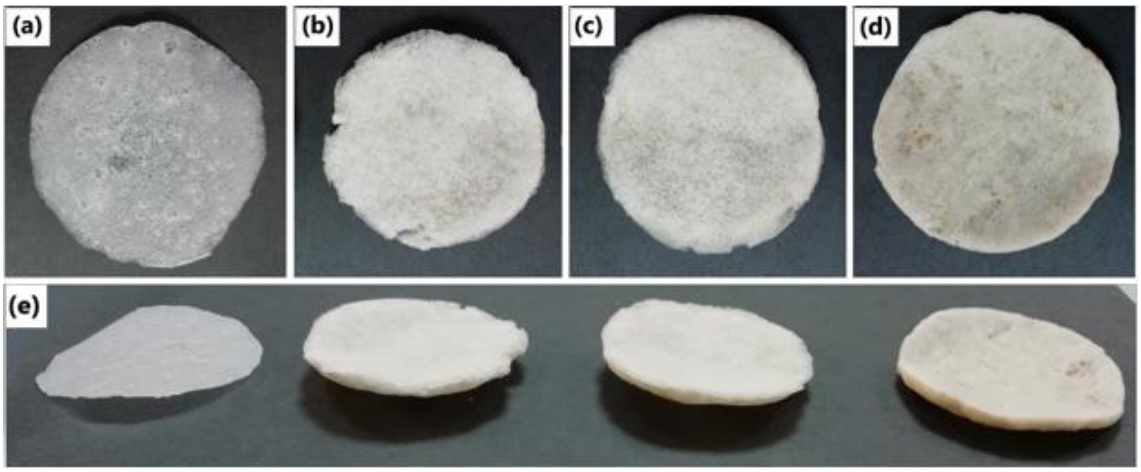

Figure 3.7. Top views of (a) MF-0, (b) MF-5, (c) MF-10, (d) MF-20 and (e) side view of all foams

A nonporous skin layer was formed on one side of all synthesized foam samples. During the depressurization stage of the foaming process, the gas molecules are

desorbed from the surface of the polymeric sample. The surface of sample can not nucleate owing to a lack of enough quantity of dissolved gas molecules. Such foams are generally known as "integral foams" and have a porous core and a nonporous skin layer [137]. Integral foams are encountered in batch, extrusion and injection molding foaming techniques [104]. In the literature, it is possible to find many studies in which integral foams are obtained [109,138-140].

3.7. Oil Absorption Capacity Tests for the Foam Absorbents

3.7.1. Determination of the oil absorption capacity of foam absorbents

The oil absorption capacity of the foamed samples synthesized from both blank LDPE and its composites containing 5wt.%, 10 wt.% and 20wt.% of organosepiolite was determined for olive oil, diesel, gasoline and waste olive oil as water pollutant. All of the oil absorption experiments were carried out in pure oil mediums. The main purpose of the experiments was to determine the absorption capacity of each synthesized foam for different types of oils and reveal the optimum synthesis conditions, namely, the foaming pressure and the organosepiolite content.

The results of the oil absorption experiments for pure oil mediums were visualized in Figure 3.8, where the oil absorption capacity was plotted against the saturation pressure of the foamed samples. The absorption capacity of the foamed samples was significantly depended on the saturation pressure, organoclay content and the type of oil used as pollutant.

Generally, the highest oil absorption performances were achieved when olive oil was used as pollutant and the absorption capacity of the foams was significantly decreased in diesel and gasoline. The viscosity of olive oil and waste oil is considerably higher compared to diesel and gasoline. Although, the higher oil viscosity decreses the rate of oil absorption, it increases the retention capability of oil within the foam [38,141]. Therefore, olive oil retained within the pores of the foam samples more than diesel and gasoline, which allowed the foams to exhibit higher oil absorption performance.

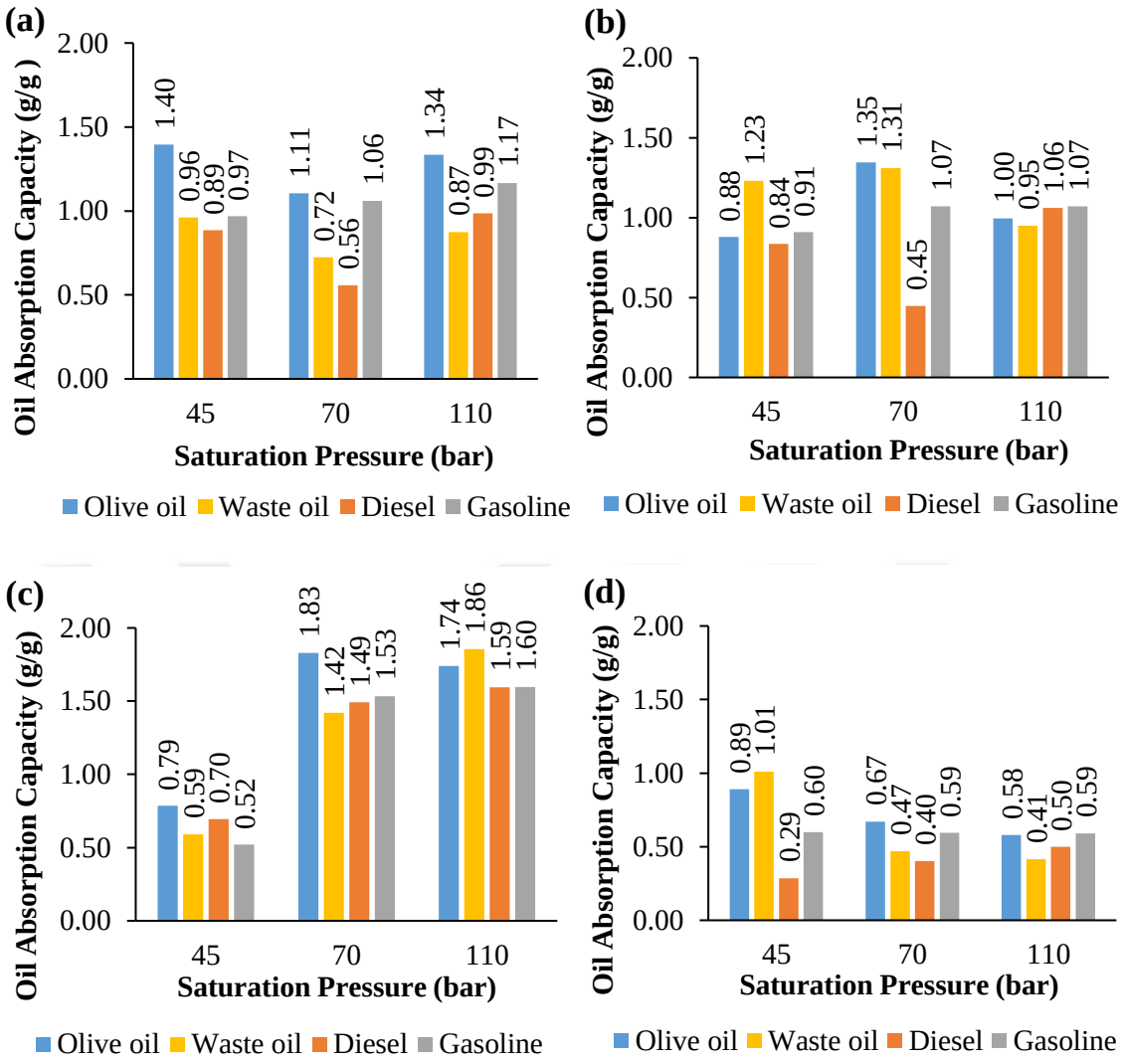

Figure 3.8. The absorption capacity of the foam samples with (a) blank, (b) 5 wt%, (c) 10 wt% and (d) 20 wt% organosepiolite content

In foaming process, the use of organosepiolite allowed to control the foam morphology. According to the oil absorption experiments, the optimum amount of organosepiolite in the foamed samples was determined as 10 wt.%. The addition of up to 10 wt.% of organoclay improved the strength and the cell structure of the foam, which increased its ability to retain oil in its structure. However, the addition of organosepiolite higher than 10 wt.% restain the cell formation and cause to reduction in the total surface area of the foams. As a result of the reduction in the total surface area, the foams significantly lost their oil absorption abilities, which leaded the foams containing 20 wt.% organosepiolite to exhibit lower oil absorption performance [37]. As seen in Figure 3.8c, the highest oil absorption performances were achieved with both saturation

pressures at 70 bar and 110 bar. Since similar oil absorption performances were achieved with both the saturation pressures, the optimum saturation pressure was determined as 70 bar.

The sheets used in foam production could not be produced in a sufficiently homogeneous thickness. In addition, during the production of the sheets, air bubbles were formed because sufficient pressure was not reached. For this reason, the foams produced from these sheets did not have a uniform thickness, which significantly affected the oil absorption performances of the foams. Therefore, to improve oil absorption performances of the foams, the production conditions of the sheets were optimized.

As a result of oil absorption tests, the sample which exhibits the best oil absorption performance was determined and its process parameters were used to synthesize the final oil absorbent foam. For each type of oil, the best oil absorption performance was achieved with MF-10 foam consist 10 wt.% organosepiolite and saturated under 70 bar. All further foaming experiments were carried out with these optimum processing conditions.

3.7.2. Investigation of oil absorption capacity for the first use and the reusability feature of the MF-10 foam

Each oil absorption experiments were conducted for three specimens in pure olive oil medium and the average oil absorption capacities of MF-10 foams were recorded. After the first use of the samples, their reusability feature was investigated.

In Figure 3.9, the oil absorption capacities of both MF-10 at the first use and three subsequent reuses were presented. As expected, the highest oil absorption performances were achieved with the first use of MF-10 for all types of oil. The first oil absorption capacities of the foam were 2.85, 3.38, 3.09 and 2.82 for olive oil, waste olive oil, diesel and gasoline, respectively. As can be seen, the oil absorption capacity of MF-10 foam was noticeably improved with the optimization of the production conditions of the sheets.

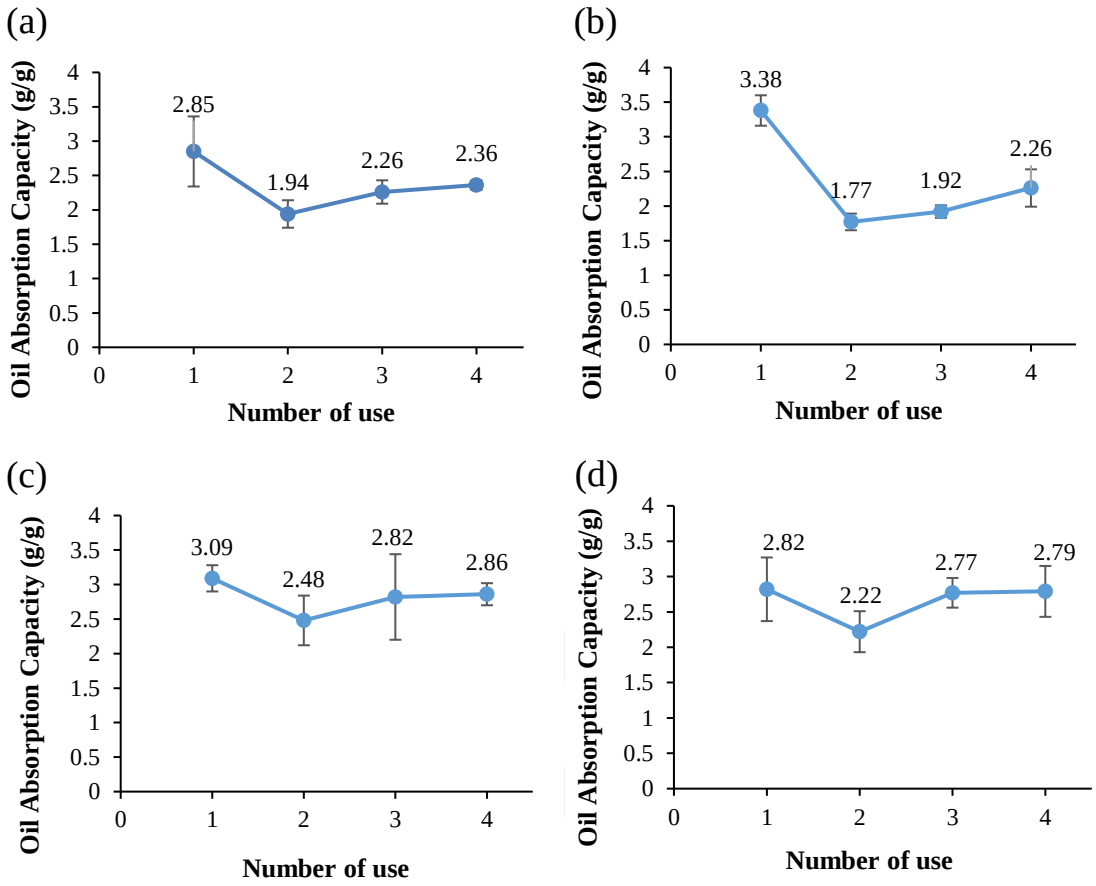

Figure 3.9. Oil absorption capacity of the foams for four successive use in (a) olive oil, (b) waste oil, (c) diesel and (d) gasoline

Reusability of the absorbents can be considered one of the most important properties of a good absorbent material. The reusability of absorbents not only reduces the cost of oil clean up, but also contributes to the notable reduction of the formation of solid waste [142]. The reusability feature of MF-10 foam was investigated by repeated three further absorption-desorption cycles after the first usage. The experiments were conducted for three specimens cut from each entire foam for three cycles and for each reuse the mean results were obtained. The change in the absorption capacity of the absorbent during four reuse cycles was presented in Figure 3.9. As can be seen, after initial use the absorption capacity of the foam decreased. This can be attributed to both the incomplete removal of oil from the foam and the partial destruction of the cellular foam structure. Despite a decrease in oil absorption capacity after first use, oil absorption performance remained stable over subsequent uses. In total, about 9.41 g olive oil, 9.33 g waste olive oil, 11.25 g diesel and 10.6 g gasoline were recovered from four successive use of the

same foam sample. The results of the reusability experiments clearly showed that, the flexible nature of the foam absorbent makes possible the high reusability of the foam with stable oil absorption performance. Therefore, MF-10 foam can be efficiently used as oil absorbent.

3.7.3. The oil absorption capacity experiments of MF-0 and MF-10 foams in the simulated oil-sea water systems

The oil absorption capacity the MF-0 and MF-10 foams was determined for four different oil-sea water systems. Olive oil, waste olive oil, diesel oil and gasoline were used as oil pollutants. The experiments were conducted in olive oil-sea water system is given in Figure 3.10.

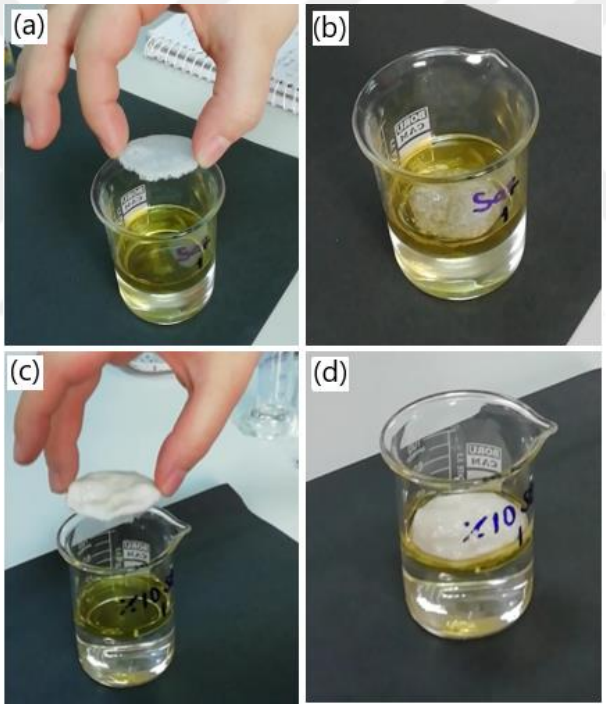

Figure 3.10. (a) MF-0 foam and olive oil-water system before oil absorption, (b) MF-0 foam and olive oil-water system after oil absorption, (c) MF-10 foam and olive oil-water system before oil absorption, (d) MF-10 foam and olive oil-water system after oil absorption

As shown in Figure 3.11, the oil absorption capacity increased significantly for each oil type with the addition of 10% by weight of organosepiolite to the matrix structure compared to the blank LDPE foam. The increase in absorption capacity was 3.8, 5.7, 5.7

and 8.4 times for olive oil, waste olive oil, diesel and gasoline, respectively. Both foams were absorbed olive oil and waste olive oil more than diesel and gasoline similar to the results obtained from pure olive oil medium. Olive oil and waste olive oil with higher viscosity were retained more in the foams than diesel and gasoline, thus the foams exhibited higher oil absorption performance in these oils. As a result, the best oil absorption performance was achieved with MF-10 foam as 3.31 g/g for the removal of waste oil from water surface.

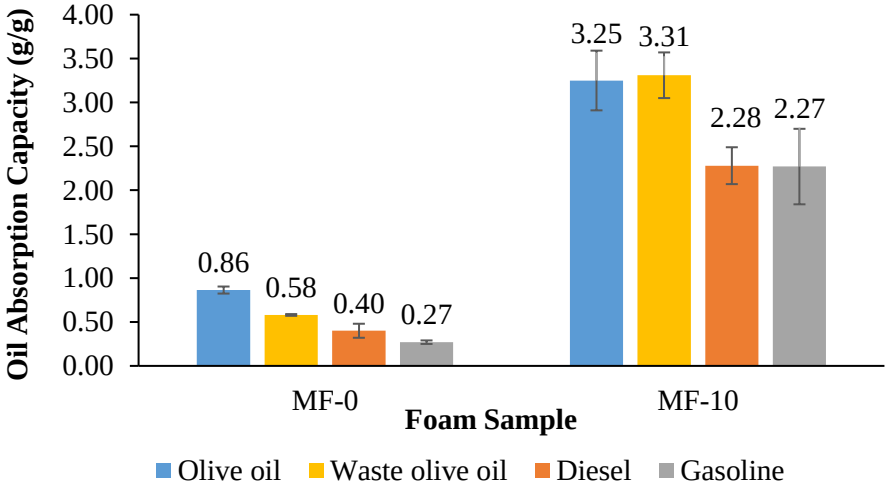

Figure 3.11. The oil absorption capacities of MF-0 and MF-10 foams in four different simulated oil-sea water systems.

In literature, many different type of oil absorbent foams were synthesized with different materials and the synthesis methods (Table 3.3). In general, literature studies have focused on the synthesis of polyurethane based foams. Nikkhah et al. (2015) synthesized polyurethane-closite 20A nanoclay nanocomposite foams by chemical foaming method for oil removal applications. The maximum oil absorption capacity was achieved with the addition of 3 wt.% nanoclay to the polymer matrix as 21.5 g/g for light crude oil. Santos et al. (2017) synthesized polyurethane foam by chemical foaming method. They obtained the maximum oil absorption capacity for crude oil as 29.8 g/g. Apart from polyurethane foams, different polymer foams were also synthesized to be used in oil removal applications. Hou et al. (2019) synthesized polypropylene foam by batch foaming method under 20 MPa of foaming pressure and 135°C of foaming temperature. They obtained the volume expansion ratio of the foam as 23.9. The oil absorption capacity of the foam was reported as 17.0 g/g and 19.9 g/g for silicone oil

and peanut oil, respectively. To the best our knowledge, there is no study about the synthesis of LDPE-silylated sepiolite composite foam and its usage in oil removal applications from water surface. Therefore, there is no result that can be compared with the oil absorption capacity of MF-10 synthesized in this study. Compared to other foam materials in literature, the oil absorption of the synthesized foam is low. The main reason of this is that the volume expansion ratio (i.e. 7.43) of the foam was lower than those of other studies.

Table 3.3. Oil absorption capacities of some foam materials reported in other studies.

Oil Absorbent	Synthesis method	Oil studied	Oil absorption capacity	Reference
Polypropylene foam	Batch foaming	Silicone oil Peanut oil	17.0 19.9	[36]
Polyurethane/Closite 20A (3 wt.%) nanocomposite foam	Chemical foaming	Light crude oil	21.5	[37]
Polyurethane foam	Chemical foaming	Diesel Gasoline Motor oil Kerosene Crude oil	16.8 15.7 20.7 25.4 29.8	[113]
Polypropylene/polyolefin elastomer (30 wt.%) blend foam	Extrusion foaming	Motor oil Bean oil	15.1 19.9	[143]
Polyurethane/activated carbon (1 wt.%) foam	Chemical foaming	Light crude oil	27.15	[144]
Polyurethane/lignin (10 wt.%) composite foam	Chemical foaming	Crude oil	28.9	[145]
Polypropylene/ polytetrafluoroethylene (3 wt.%) blend foam	Extrusion foaming	Octane Gasoline Light crude oil Diesel Heavy crude oil Kerosene	26.1 24.2 14.7 12.6 8.4 6.6	[146]

3.8. Characterization of the Foam Absorbents

3.8.1. The density and the volume expansion ratio of the foams

The density of the sheets (ρ_o), the density (ρ_f) and the volume expansion ratio (R_f) of the foams were given in Table 3.4. As expected, the density of the sheets increased with increasing organosepiolite content, while the density of all foams decreased with the effect of the volume expansion. LDPE and the composite foams were demonstrated different volume expansion ratios depending on their varying organosepiolite content. MF-0 showed the least volume expansion ratio as 1.55. The volume expansion ratio was increased to 5.71 with the addition of 5% by weight of organosepiolite, and the volume expansion ratio reached the maximum value of 7.43 with the addition of 10% by weight organosepiolite. The expansion ratio considerably reduced with further increasing of filler content in the matrix.

Table 3.4. The density of the sheets (ρ_o), the density (ρ_f) and the volume expansion ratio (R_f) of the foams for different organosepiolite content

Organosepiolite Content of Samples (wt.%)	Density of the Sheets (ρ_o)	Density of the Foams (ρ_f)	Volume Expansion Ratio of Foams (R_f)
0	0.79	0.51	1.55
5	0.82	0.14	5.71
10	0.85	0.11	7.43
20	0.87	0.23	3.85

In Figure 3.12, CS-10 sheet and its foam, MF-10, was presented. As seen, the volume expansion of the composite material from the sheet to the foam form is clearly visible from the image.

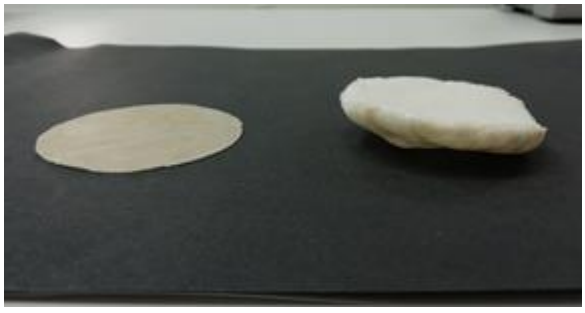

Figure 3.12. The images of CS-10 composite sheet and its foam, MF-10

3.8.2. Scanning electron microscopy (SEM) analysis

To observe the effect of organosepiolite content in the matrix on the cellular morphology, foamed LDPE and foamed composites with different weight percent of organosepiolite were analyzed by a scanning electron microscopy (SEM). As known, cell nucleation can be generated either by "homogeneous nucleation" or "heterogeneous nucleation" mechanisms. In homogeneous nucleation, the polymeric material does not contain any foreign bodies. Concordantly, cell nucleation occurs randomly and spontaneously. In heterogoneous nucleation, the polymer contains foreign bodies that serve as sites for cell nucleation. These sites act as nucleation agent by creating locations for cell formation and restricting cell expansion during the foaming process, which leads to decreased cell size and improved cell structure [102,107].

As seen in the SEM microphotographs, the cell morphology of the foams was significantly affected by the change in the organosepiolite content of the foams. Accordingly, as seen in Figure 3.13a and b, the blank LDPE foam exhibited non-uniform and the most distorted cell structure due to the lack of nucleation sites. Consequently, the lowest volume expansion ratio was calculated for MF-0 foam as 1.55. With the addition of 5 wt.% organosepiolite to the LDPE matrix, cell structures were noticeably improved compared to MF-0 and the volume expansion increased about 3.7 fold reaching as high as 5.74 (Figure 3.13c and d). However, as seen in these figures, 5 wt.% of filler content was not sufficient for the improvement of cell structures, and some cells were still in a defective structure. With the addition of 10 wt.% organosepiolite to the LDPE matrix, the structure of cells was improved, significantly. MF-10 foam exhibited the highest volume expansion ratio (i.e. 7.43) having increased about 4.8 folds compared to MF-0 (Figure 3.13e and f). When the organosepiolite content in the matrix was increased to 20 wt.%, MF-20 foam exhibited non-uniform and distorted cell structure again. Both cell nucleation was restricted by the excess filler content and, the filler particles coalesced to larger diameters leading to the formation of non-uniform cell nucleation sites for foaming process (Figure 3.13g and h). Although, a significant decrease in the volume expansion ratio was observed for MF-20 with respect to MF-10, the expansion was still approximately 2.5 times higher than MF-0. Therefore, the existence of any organosepiolite content in matrix reduced cell size compared to the blank foam, leaded to lower foam density and thus higher expansion ratio [104,114].

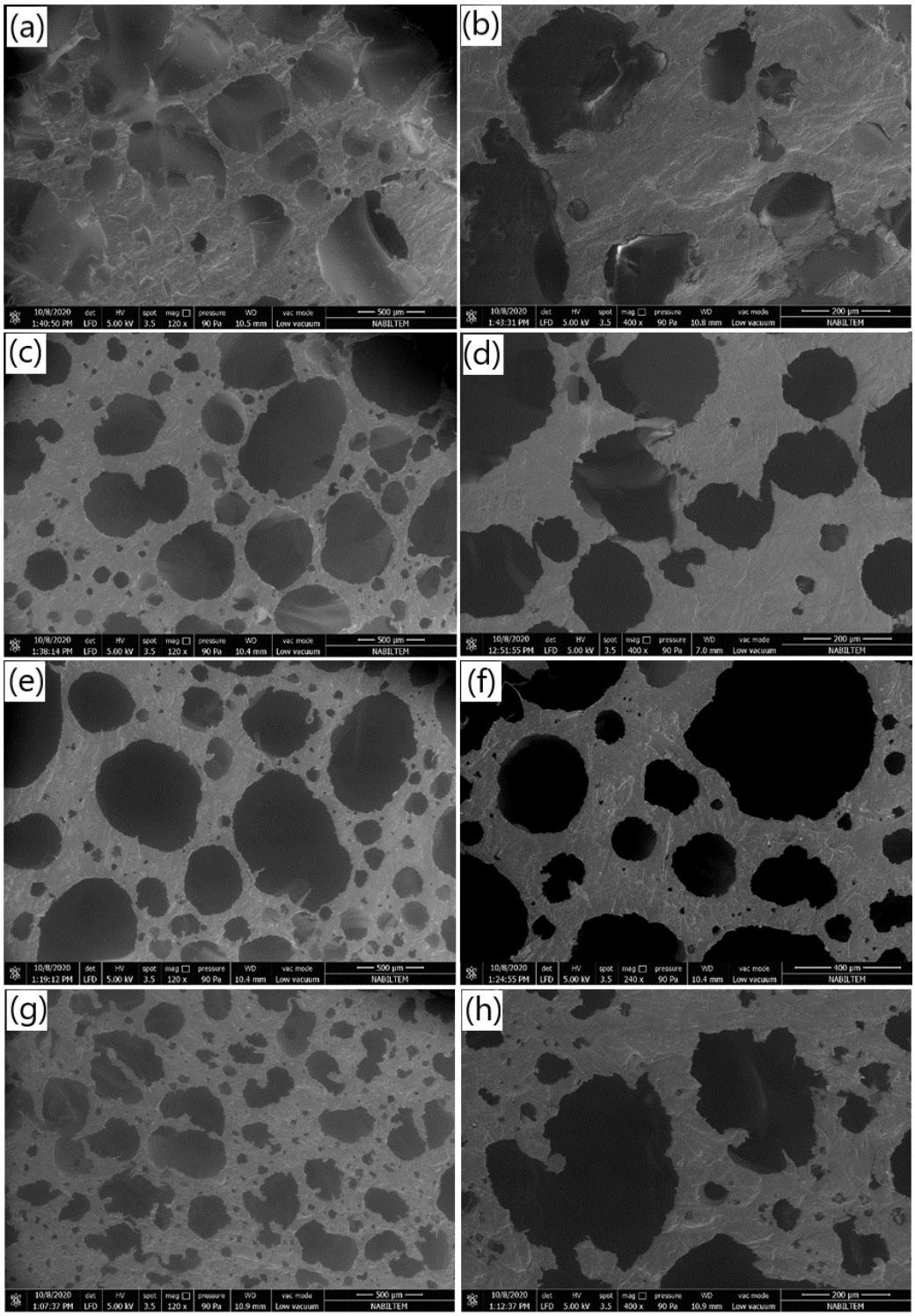

Figure 3.13. SEM micrographs of (a) MF-0 under the magnification of 120×, (b) MF-0 under the magnification of 400×, (c) MF-5 under the magnification of 120×, (d) MF-5 under the magnification of 400×, (e) MF-10 under the magnification of 120×, (f) MF-10 under the magnification of 240×, (g) MF-20 under the magnification of 120×,and (h) MF-20 under the magnification of 400×.

3.8.3. Water Contact Angle Measurements

The surface properties of a solid material can be classified by the contact angle between the water droplet surface and the solid surface. The contact angle (θ) can be described as the angle between the liquid drop surface and the solid surface and reflects the degree of wettability of the surface. 0° and 180° contact angle values indicate two separate endpoints for wetting behaviour of a material. While the contact angle of 0° demonstrates that the solid surface is completely wetted by the liquid, the contact angle of 180° demonstrates that the solid surface is no wetted by the liquid [147]. The water contact angle less than 90° refers to hydrophilic surface properties. In such surfaces, water droplets easily spread out on the surface of the material. The contact angle of higher than 90° refers to hydrophobic surface properties. In Figure 3.14, such surfaces with their contact angles were presented [148].

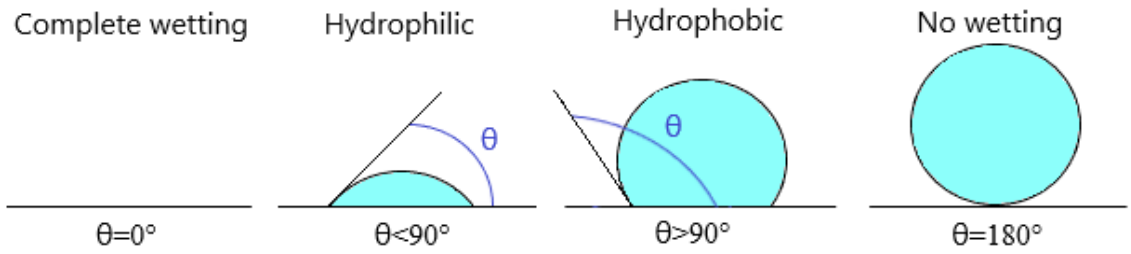

Figure 3.14. Schematics of contact angles on different solid surfaces [148].

The water contact angle measurements were carried out to determine the surface characteristics of the foams. The water contact angle of MF-10 was found as 75° indicating hydrophilic surface properties, while that of MF-20 was found as 120° indicating hydrophobic surface properties. Although the MF-10 shows the best oil absorption performance, it exhibited the hydrophilic surface angle. As seen in Figure 3.15, MF-20 foam surface was characterized with non-uniform pores with smaller pore openings while MF-10 exhibited pores with relatively larger diameters. As a result, the water droplets entered the foam holes of MF-10 and the contact angle was reduced. Although the MF-20 shows the lowest oil absorption performance, it exhibited the hydrophobic surface angle. The main reason of this may be that the surface of MF-20 foam was smoother than MF-10, due to cell nucleation limited by the excess filler content.

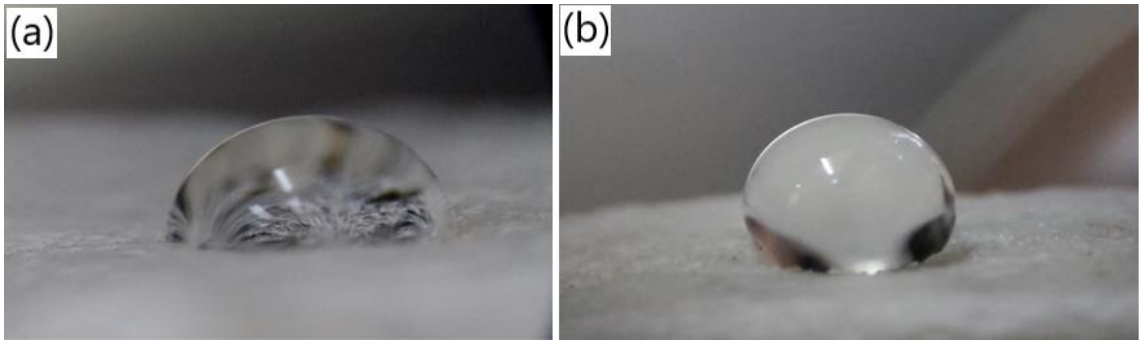

Figure 3.15. The images of a drop of water on (a) MF-10 foam and (b) MF-20 foam

4. CONCLUSIONS

In this thesis, the organosepiolite samples were first produced for composite material production and then a series of LDPE and the composite foams with different weight percent of organosepiolite were synthesized, characterized, and tested for their oil absorption capacities in both pure oil and oil-water media. The composite foams were produced by pressure induced technique of the batch foaming method. The experimental results demonstrated that the 10 wt.% organosepiolite-LDPE composite foam produced at 70 bar showed the best oil absorption performance for oil clean up both in pure oil and oil-water media. Both in pure oil and simulated sea water-oil media, the best absorption performances were achieved with waste olive oil as 3.38 g/g and 3.31 g/g. Reusability experiments have shown that the oil absorption capacities of the samples are not significantly affected by repeated absorption-squeezing cycles after first use due to the flexible nature of the foams. With 10 wt.% filler content of MF-10, the highest volume expansion ratio was achieved as 7.43, which was about 4.8 fold of that of MF-0. The SEM microphotographs also confirm the change in the foam morphology with the varying organosepiolite contents. MF-0 showed non-uniform and the most distorted cell structure due to the lack of nucleation sites. With the addition of 10 wt.% organosepiolite to the LDPE matrix, the structure of cells was significantly improved, which explained the superiority of oil absorption capacity of MF-10 over that of MF-0, MF-5, and MF-20. Thus, MF-10 composite foam synthesized from recycled LDPE as the main phase and silane (GPTMS) modified sepiolite as the filler is proposed as an efficient and reusable oil absorbent material from aqueous media. The mechanical properties of composite foams could not be studied due to the lack of a suitable device. Therefore, it is recommended that the product should be subjected to mechanical tests before its use.

REFERENCES

[1] World Wildlife Fund for Nature (WWF) (2014) Türkiye'nin Su Riskleri Raporu, https://wwftr.awsassets.panda.org/downloads/turkiyenin_su_riskleri__raporu_web.pdf?4180 (16.09.2019).

[2] TMMOB Çevre Mühendisleri Odası (2018) Dünya Çevre Günü Türkiye Raporu, http://www.cmo.org.tr/resimler/ekler/0d4a5b926c005a6_ek.pdf (16.09.2019).

[3] Singh, N. B., Nagpal, G., Agrawal, S.,Rachna. (2018) Water purification by using Adsorbents: A Review. Environmental Technology & Innovation, 11, 187-240.

[4] Mysore, D., Viraraghavan, T.,Jin, Y. C. (2005) Treatment of oily waters using vermiculite. Water Research, 39(12), 2643-2653.

[5] Group of Experts on the Scientific Aspects of Marine Environmental Protection (GESAMP) (2007) Estimates of Oil Entering the Marine Environment from Sea-Based Activities, http://www.gesamp.org/site/assets/files/1257/estimates-of-oil-entering-the-marine-environment-from-sea-based-activities-en.pdf (29.12.2018).

[6] An, C., Huang, G., Yao, Y.,Zhao, S. (2017) Emerging usage of electrocoagulation technology for oil removal from wastewater: A review. Science of the Total Environment, 579, 537-556.

[7] Soto-Oñate, D.,Caballero, G. (2017) Oil spills, governance and institutional performance: The 1992 regime of liability and compensation for oil pollution damage. Journal of Cleaner Production, 166, 299-311.

[8] The International Tanker Owners Pollution Federation Limited (ITOPF) (2019) Oil Tanker Spill Statics 2018, https://www.itopf.org/fileadmin/data/Documents/Company_Lit/Oil_Spill_Stats_2019.pdf (03.09.2019).

[9] Ünlü S., Alpar, B., Öztürk, B. (2018) Oil Spill along the Turkish Straits Sea Area; Accidents, Environmental Pollution, Socio-Economic Impacts and Protection, http://tudav.org/wp-content/uploads/2018/12/Oil_Spill_Book_2018_TUDAV.pdf (20.05.2019).

[10] The International Tanker Owners Pollution Federation Limited (ITOPF) (2014) Effects of Oil Pollution on the Marine Environment, https://www.itopf.org/fileadmin/data/Documents/TIPS%20TAPS/TIP_13_Effect

s_of_Oil_Pollution_on_the_Marine_Environment.pdf (18.09.2019).

[11] The International Tanker Owners Pollution Federation Limited (ITOPF) (2014) Effects of Oil Pollution on Fisheries and Mariculture, https://www.itopf.org/fileadmin/data/Documents/TIPS%20TAPS/TIP_11_Effects_of_Oil_Pollution_on_Fisheries_and_Mariculture.pdf (18.09.2019).

[12] Bayat, A., Aghamiri, S. F., Moheb, A.,Vakili-Nezhaad, G. R. (2005) Oil Spill Cleanup from Sea Water by Sorbent Materials. Chemical Engineering & Technology, 28(12), 1525-1528.

[13] Dave, D.,Ghaly, A. E. (2011) Remediation Technologies for Marine Oil Spills: A Critical Review and Comparative Analysis. American Journal of Environmental Sciences, 7(5), 423-440.

[14] Li, P., Cai, Q., Lin, W., Chen, B.,Zhang, B. (2016) Offshore oil spill response practices and emerging challenges. Marine Pollution Bulletin, 110(1), 6-27.

[15] Venkatanarasimhan, S.,Raghavachari, D. (2013) Epoxidized natural rubber–magnetite nanocomposites for oil spill recovery. Journal of Materials Chemistry A, 1(3), 868-876.

[16] The International Tanker Owners Pollution Federation Limited (ITOPF) (2014) Use of Booms in Oil Pollution Response, https://www.itopf.org/fileadmin/data/Documents/TIPS%20TAPS/TIP_3_Use_of_Booms_in_Oil_Pollution_Response.pdf (18.09.2019).

[17] The International Tanker Owners Pollution Federation Limited (ITOPF) (2014) Use of Skimmers in Oil pollution Response, https://www.itopf.org/fileadmin/data/Documents/TIPS%20TAPS/TIP_5_Use_of_Skimmers_in_Oil_Pollution_Response.pdf (18.09.2019).

[18] Al-Majed, A. A., Adebayo, A. R.,Hossain, M. E. (2012) A sustainable approach to controlling oil spills. Journal of Environmental Management, 113, 213-227.

[19] Ge, J., Zhao, H. Y., Zhu, H. W., Huang, J., Shi, L. A.,Yu, S. H. (2016) Advanced Sorbents for Oil-Spill Cleanup: Recent Advances and Future Perspectives. Advanced Materials, 28(47), 10459-10490.

[20] Motta, F. L., Stoyanov, S. R.,Soares, J. B. P. (2018) Application of solidifiers for oil spill containment: A review. Chemosphere, 194, 837-846.

[21] Galán, E. (1996) Properties and Applications of Palygorskite-Sepiolite Clays.

Clay Minerals, 31, 443-453.

[22] The International Tanker Owners Pollution Federation Limited (ITOPF) (2014) Use of sorbent materials in oil spill response, https://www.itopf.org/fileadmin/data/Documents/TIPS%20TAPS/TIP_8_Use_of_Sorbent_Materials_in_Oil_Spill_Response.pdf (18.09.2019).

[23] Wahi, R., Chuah, L. A., Choong, T. S. Y., Ngaini, Z.,Nourouzi, M. M. (2013) Oil removal from aqueous state by natural fibrous sorbent: An overview. Separation and Purification Technology, 113, 51-63.

[24] Saleem, J., Adil Riaz, M.,Gordon, M. (2018) Oil sorbents from plastic wastes and polymers: A review. Journal of Hazardous Materials, 341, 424-437.

[25] Zhu, H., Qiu, S., Jiang, W., Wu, D.,Zhang, C. (2011) Evaluation of electrospun polyvinyl chloride/polystyrene fibers as sorbent materials for oil spill cleanup. Environmental Science & Technology, 45(10), 4527-4531.

[26] Singh, V., Kendall, R. J., Hake, K.,Ramkumar, S. (2013) Crude Oil Sorption by Raw Cotton. Industrial & Engineering Chemistry Research, 52(18), 6277-6281.

[27] Deschamps, G., Caruel, H., Borredon, M.-E., Bonnin, C.,Vignoles, C. (2003) Oil Removal from Water by Selective Sorption on Hydrophobic Cotton Fibers. 1. Study of Sorption Properties and Comparison with Other Cotton Fiber-Based Sorbents. Environmental Science & Technology, 37(5), 1013-1015.

[28] Choi, H. M.,Cloud, R. M. (1992) Natural sorbents in oil spill cleanup. Environmental Science & Technology, 26(4), 772-776.

[29] Nwadiogbu, J. O., Ajiwe, V. I. E.,Okoye, P. A. C. (2016) Removal of crude oil from aqueous medium by sorption on hydrophobic corncobs: Equilibrium and kinetic studies. Journal of Taibah University for Science, 10(1), 56-63.

[30] Srinivasan, A.,Viraraghavan, T. (2008) Removal of oil by walnut shell media. Bioresource Technology, 99(17), 8217-8220.

[31] Rengasamy, R. S., Das, D.,Karan, C. P. (2011) Study of oil sorption behavior of filled and structured fiber assemblies made from polypropylene, kapok and milkweed fibers. Journal of Hazardous Materials, 186(1), 526-532.

[32] Abdelwahab, O. (2014) Assessment of raw luffa as a natural hollow oleophilic fibrous sorbent for oil spill cleanup. Alexandria Engineering Journal, 53(1), 213-218.

[33] Banerjee, S. S., Joshi, M. V.,Jayaram, R. V. (2006) Treatment of oil spill by sorption technique using fatty acid grafted sawdust. Chemosphere, 64(6), 1026-1031.

[34] Adebajo, M., Frost, R., Kloprogge, T., Carmody, O.,Kokot, S. (2003) Porous Materials for Oil Spill Cleanup: A Review of Synthesis and Absorbing Properties. Journal of Porous Materials, 10, 159-170.

[35] Saleem, J., Ning, C., Barford, J.,McKay, G. (2015) Combating oil spill problem using plastic waste. Waste Management, 44, 34-38.

[36] Hou, J., Zhao, G., Zhang, L., Wang, G.,Li, B. (2019) High-expansion polypropylene foam prepared in non-crystalline state and oil adsorption performance of open-cell foam. Journal of Colloid and Interface Science, 542, 233-242.

[37] Nikkhah, A. A., Zilouei, H., Asadinezhad, A.,Keshavarz, A. (2015) Removal of oil from water using polyurethane foam modified with nanoclay. Chemical Engineering Journal, 262, 278-285.

[38] Ceylan, D., Dogu, S., Karacik, B., Yakan, S. D., Okay, O. S.,Okay, O. (2009) Evaluation of Butyl Rubber as Sorbent Material for the Removal of Oil and Polycyclic Aromatic Hydrocarbons from Seawater. Environmental Science & Technology, 43(10), 3846-3852.

[39] Ji, F., Li, C., Dong, X., Li, Y.,Wang, D. (2009) Separation of oil from oily wastewater by sorption and coalescence technique using ethanol grafted polyacrylonitrile. Journal of Hazardous Materials, 164(2-3), 1346-1351.

[40] Lin, C., Huang, C.-L.,Shern, C.-C. (2008) Recycling waste tire powder for the recovery of oil spills. Resources, Conservation and Recycling, 52(10), 1162-1166.

[41] Li, Y., Wang, M., Sun, D., Li, Y.,Wu, T. (2018) Effective removal of emulsified oil from oily wastewater using surfactant-modified sepiolite. Applied Clay Science, 157, 227-236.

[42] Zadaka-Amir, D., Bleiman, N.,Mishael, Y. G. (2013) Sepiolite as an effective natural porous adsorbent for surface oil-spill. Microporous and Mesoporous Materials, 169, 153-159.

[43] Moazed, H.,Viraraghavan, T. (2005) Removal of Oil from Water by Bentonite

Organoclay. Practice Periodical of Hazardous, Toxic, and Radioactive Waste Management, 9, 130-134.

[44] Bastani, D., Safekordi, A. A., Alihosseini, A.,Taghikhani, V. (2006) Study of oil sorption by expanded perlite at 298.15K. Separation and Purification Technology, 52(2), 295-300.

[45] Ayotamuno, M. J., Kogbara, R. B., Ogaji, S. O. T.,Probert, S. D. (2006) Petroleum contaminated ground-water: Remediation using activated carbon. Applied Energy, 83(11), 1258-1264.

[46] Inagaki, M., Konno, H., Toyoda, M., Moriya, K.,Kihara, T. (2000) Sorption and recovery of heavy oils by using exfoliated graphite Part II: Recovery of heavy oil and recycling of exfoliated graphite. Desalination, 128(3), 213-218.

[47] Mohd Zaini, N. A., Ismail, H.,Rusli, A. (2017) Short Review on Sepiolite-Filled Polymer Nanocomposites. Polymer-Plastics Technology and Engineering, 56(15), 1665-1679.

[48] Tournassat, C., Bourg, I.C., Steefel, C.I., Bergaya, F. (2015) Developments in Clay Science, 6, 1st Edition, Elsevier.

[49] Wythers, M.C. (2014) Advances in Materials Science Research, 17, Nova Science Publishers, Inc, New York, USA.

[50] Tian, G., Han, G. Wang, F., Liang, J. (2019) Sepiolite Nanomaterials: Structure, Properties and Functional Applications, Nanomaterials from Clay Minerals: A New Approach to Green Functional Materials, Elsevier.

[51] Galàn E., Singer, A. (2011) Developments in Clay Science, 3, 1st Edition, Elsevier.

[52] Akçay, M. (2004) FT-IR spectroscopic investigation of the adsorption pyridine on the raw sepiolite and Fe-pillared sepiolite from anatolia. Journal of Molecular Structure, 694(1), 21-26.

[53] Karakashev, S. I., Ozdemir, O., Hampton, M. A.,Nguyen, A. V. (2011) Formation and stability of foams stabilized by fine particles with similar size, contact angle and different shapes. Colloids and Surfaces A: Physicochemical and Engineering Aspects, 382(1), 132-138.

[54] Zhou, C. H., Li, G. L., Zhuang, X. Y., Wang, P. P., Tong, D. S., Yang, H. M., Lin, C. X., Li, L., Zhang, H., Ji, S. F.,Yu, W. H. (2017) Roles of texture and

acidity of acid-activated sepiolite catalysts in gas-phase catalytic dehydration of glycerol to acrolein. Molecular Catalysis, 434, 219-231.

[55] Tartaglione, G., Tabuani, D.,Camino, G. (2008) Thermal and morphological characterisation of organically modified sepiolite. Microporous and Mesoporous Materials, 107(1-2), 161-168.

[56] Balci, S. (1999) Effect of heating and acid pre-treatment on pore size distribution of sepiolite. Clay Minerals, 34(4), 647-655.

[57] Mora, M., Isabel López, M., Ángeles Carmona, M., Jiménez-Sanchidrián, C.,Rafael Ruiz, J. (2010) Study of the thermal decomposition of a sepiolite by mid- and near-infrared spectroscopies. Polyhedron, 29(16), 3046-3051.

[58] Marjanović, V., Lazarević, S., Janković-Častvan, I., Potkonjak, B., Janaćković, Đ.,Petrović, R. (2011) Chromium (VI) removal from aqueous solutions using mercaptosilane functionalized sepiolites. Chemical Engineering Journal, 166(1), 198-206.

[59] Yebra-Rodríguez, A., Martín-Ramos, J. D., Rey, F. d., Viseras, C.,López-Galindo, A. (2003) Effect of acid treatment on the structure of sepiolite. Clay Minerals, 38(3), 353-360.

[60] de Paiva, L. B., Morales, A. R.,Valenzuela Díaz, F. R. (2008) Organoclays: Properties, preparation and applications. Applied Clay Science, 42(1), 8-24.

[61] Zou, H., Wu, S.,Shen, J. (2008) Polymer/Silica Nanocomposites: Preparation, Characterization, Properties, and Applications. Chemical Reviews, 108(9), 3893-3957.

[62] Zare, Y. (2016) The roles of nanoparticles accumulation and interphase properties in properties of polymer particulate nanocomposites by a multi-step methodology. Composites Part A: Applied Science and Manufacturing, 91, 127-132.

[63] Fu, S.-Y., Feng, X.-Q., Lauke, B.,Mai, Y.-W. (2008) Effects of particle size, particle/matrix interface adhesion and particle loading on mechanical properties of particulate–polymer composites. Composites Part B: Engineering, 39(6), 933-961.

[64] Olad, A. (2011) Polymer/Clay Nanocomposites, Advances in Diverse Industrial Applications of Nanocomposites, 113-138,

https://www.intechopen.com/books/advances-in-diverse-industrial-applications-of-nanocomposites/polymer-clay-nanocomposites (20.04.2020).

[65] Jesson, D. A.,Watts, J. F. (2012) The Interface and Interphase in Polymer Matrix Composites: Effect on Mechanical Properties and Methods for Identification. Polymer Reviews, 52(3), 321-354.

[66] Kato, M., Okamoto, H., Hasegawa, N., Tsukigase, A.,Usuki, A. (2003) Preparation and Properties of Polyethylene-Clay Hybrids. Polymer Engineering & Science, 43, 1312-1316.

[67] Ashraf, M. A., Peng, W., Zare, Y.,Rhee, K. Y. (2018) Effects of Size and Aggregation/Agglomeration of Nanoparticles on the Interfacial/Interphase Properties and Tensile Strength of Polymer Nanocomposites. Nanoscale Research Letters, 13(1), 214-214.

[68] Nguyen, Q.,Baird, D. (2006) Preparation of Polymer–Clay Nanocomposites and their Properties. Advances in Polymer Technology, 25, 270-285.

[69] Harrats, C.,Groeninckx, G. (2008) Features, Questions and Future Challenges in Layered Silicates Clay Nanocomposites with Semicrystalline Polymer Matrices. Macromolecular Rapid Communications, 29(1), 14-26.

[70] Kango, S., Kalia, S., Celli, A., Njuguna, J., Habibi, Y.,Kumar, R. (2013) Surface modification of inorganic nanoparticles for development of organic–inorganic nanocomposites-A review. Progress in Polymer Science, 38(8), 1232-1261.

[71] Raji, M., Mekhzoum, M. E. M., Rodrigue, D., Qaiss, A. e. k.,Bouhfid, R. (2018) Effect of silane functionalization on properties of polypropylene/clay nanocomposites. Composites Part B: Engineering, 146, 106-115.

[72] Mazloom Jalali, A., Afshar Taromi, F., Atai, M.,Solhi, L. (2016) Effect of reaction conditions on silanisation of sepiolite nanoparticles. Journal of Experimental Nanoscience, 11(15), 1171-1183.

[73] Bernardo, V., Martín-de León, J., Laguna-Gutiérrez, E.,Rodríguez-Pérez, M. Á. (2017) PMMA-sepiolite nanocomposites as new promising materials for the production of nanocellular polymers. European Polymer Journal, 96, 10-26.

[74] Hernández, K. (2016) Polymer-Clay Nanocomposites and Composites: Structures, Characteristics, and their Applications in the Removal of Organic Compounds of Environmental Interest. Medicinal Chemistry, 6(3), 201-210.

[75] Nikolic, M. S., Petrovic, R., Veljovic, D., Cosovic, V., Stankovic, N.,Djonlagic, J. (2017) Effect of sepiolite organomodification on the performance of PCL/sepiolite nanocomposites. European Polymer Journal, 97, 198-209.

[76] García-López, D., Fernández, J. F., Merino, J. C., Santarén, J.,Pastor, J. M. (2010) Effect of organic modification of sepiolite for PA 6 polymer/organoclay nanocomposites. Composites Science and Technology, 70(10), 1429-1436.

[77] Yamazaki, R., Karyu, N., Noda, M., Fujii, S.,Nakamura, Y. (2016) Quantitative measurement of physisorbed silane on a silica particle surface treated with silane coupling agents by thermogravimetric analysis. Journal of Applied Polymer Science, 133(14).

[78] Pape, P.G. (2011) Adhesion Promoters, Handbook of Adhesives and Surface Preparation Technology, Applications and Manufacturing, 1st Edition., Elsevier.

[79] Zhao, C., Feng, M., Gong, F., Qin, H.,Yang, M. (2004) Preparation and characterization of polyethylene-clay nanocomposites by using chlorosilane-modified clay. Journal of Applied Polymer Science, 93(2), 676-680.

[80] Bischoff, E., Daitx, T., Simon, D. A., Schrekker, H. S., Liberman, S. A.,Mauler, R. S. (2015) Organosilane-functionalized halloysite for high performance halloysite/heterophasic ethylene–propylene copolymer nanocomposites. Applied Clay Science, 112-113, 68-74.

[81] García, N., Guzmán, J., Benito, E., Esteban-Cubillo, A., Aguilar, E., Santarén, J.,Tiemblo, P. (2011) Surface Modification of Sepiolite in Aqueous Gels by Using Methoxysilanes and Its Impact on the Nanofiber Dispersion Ability. Langmuir, 27(7), 3952-3959.

[82] Chen, H., Lu, H., Zhou, Y., Zheng, M., Ke, C.,Zeng, D. (2012) Study on thermal properties of polyurethane nanocomposites based on organo-sepiolite. Polymer Degradation and Stability, 97(3), 242-247.

[83] Turhan, Y., Doğan, M.,Alkan, M. (2013) Characterization and Some Properties of Poly(vinyl chloride)/Sepiolite Nanocomposites. Advances in Polymer Technology, 32(S1), E65-E82.

[84] Doğan, M., Turhan, Y., Alkan, M., Namli, H., Turan, P.,Demirbaş, Ö. (2008) Functionalized sepiolite for heavy metal ions adsorption. Desalination, 230(1), 248-268.

[85] Alkan, M., Tekin, G.,Namli, H. (2005) FTIR and zeta potential measurements of sepiolite treated with some organosilanes. Microporous and Mesoporous Materials, 84(1), 75-83.

[86] Jia, Z.-R., Gao, Z.-G., Lan, D., Cheng, Y.-H., Wu, G.-L.,Wu, H.-J. (2018) Effects of filler loading and surface modification on electrical and thermal properties of epoxy/montmorillonite composite. Chinese Physics B, 27(11), 117806.

[87] Arkles, B. (2014) Silane Coupling AgentsConnecting Across Boundaries, https://www.gelest.com/themencode-pdf-viewer/?file=https://www.gelest.com/wp-content/uploads/Goods-PDF-brochures-couplingagents.pdf (15.10.2019).

[88] Valentín, J. L., López-Manchado, M. A., Posadas, P., Rodríguez, A., Marcos-Fernández, A.,Ibarra, L. (2006) Characterization of the reactivity of a silica derived from acid activation of sepiolite with silane by 29Si and 13C solid-state NMR. Journal of Colloid and Interface Science, 298(2), 794-804.

[89] Myriam, M., Suárez, M.,Martín-Pozas, J. M. (1998) Structural and Textural Modifications of Palygorskite and Sepiolite Under Acid Treatment. Clays and Clay Minerals, 46(3), 225-231.

[90] Franco, F., Pozo, M., Cecilia, J. A., Benítez-Guerrero, M., Pozo, E.,Martín Rubí, J. A. (2014) Microwave assisted acid treatment of sepiolite: The role of composition and “crystallinity”. Applied Clay Science, 102, 15-27.

[91] Di, J., Jin-quan, L., Xing-fang, Y.,Yu-lin, W. (2004) Modification of sepiolite by treatment with methyl triethoxysilane. Journal of Wuhan University of Technology-Material Science Edition, 19(1), 44-47.

[92] Vilarrasa-García, E., Cecilia, J. A., Bastos-Neto, M., Cavalcante, C. L., Azevedo, D. C. S.,Rodríguez-Castellón, E. (2017) Microwave-assisted nitric acid treatment of sepiolite and functionalization with polyethylenimine applied to CO2 capture and CO2/N2 separation. Applied Surface Science, 410, 315-325.

[93] Sabah, E.,Majdan, M. (2009) Removal of phosphorus from vegetable oil by acid-activated sepiolite. Journal of Food Engineering, 91(3), 423-427.

[94] Kara, M., Yuzer, H., Sabah, E.,Celik, M. S. (2003) Adsorption of cobalt from aqueous solutions onto sepiolite. Water Research, 37(1), 224-232.

[95] Balci, S. (1996) Thermal decomposition of sepiolite and variations in pore structure with and without acid pre-treatment. Journal of Chemical Technology & Biotechnology, 66(1), 72-78.

[96] Erdoğan Alver, B. (2018) Hydrogen adsorption on natural and sulphuric acid treated sepiolite and bentonite. International Journal of Hydrogen Energy, 43(2), 831-838.

[97] Bee, S.-L., Abdullah, M. A. A., Bee, S.-T., Sin, L. T.,Rahmat, A. R. (2018) Polymer nanocomposites based on silylated-montmorillonite: A review. Progress in Polymer Science, 85, 57-82.

[98] Sinha Ray, S.,Okamoto, M. (2003) Polymer/layered silicate nanocomposites: a review from preparation to processing. Progress in Polymer Science, 28(11), 1539-1641.

[99] Pavlidou, S.,Papaspyrides, C. D. (2008) A review on polymer–layered silicate nanocomposites. Progress in Polymer Science, 33(12), 1119-1198.

[100] Lee, L., Zeng, C., Cao, X., Han, X., Shen, J.,Xu, G. (2005) Polymer nanocomposite foams. Composites Science and Technology, 65(15-16), 2344-2363.

[101] Defonseka C. (2019) Water-Blown Cellular Polymers: A Practical Guide, 2nd Edition,Walter de Gruyter.

[102] Chen, L., Rende, D., Schadler, L. S.,Ozisik, R. (2013) Polymer nanocomposite foams. Journal of Materials Chemistry A, 1(12), 3837-3850.

[103] Mittal V. (2014) Polymer Nanocomposite Foams, 1st Edition, CRC Press.

[104] Altan, M. (2018) Thermoplastic Foams: Processing, Manufacturing, and Characterization, Recent Research in Polymerization, https://www.intechopen.com/books/advances-in-diverse-industrial-applications-of-nanocomposites/polymer-clay-nanocomposites (20.04.2020).

[105] Reglero Ruiz, J., Vincent, M., Agassant, j.-f., Sadik, T., Pillon, C.,Carrot, C. (2015) Polymer foaming with chemical blowing agents: Experiment and modeling. Polymer Engineering & Science, 55, 2018-2029.

[106] Goren, K., Chen, L., Schadler, L. S.,Ozisik, R. (2010) Influence of nanoparticle surface chemistry and size on supercritical carbon dioxide processed nanocomposite foam morphology. The Journal of Supercritical Fluids, 51(3),

420-427.

[107] Okolieocha, C., Raps, D., Subramaniam, K.,Altstädt, V. (2015) Microcellular to nanocellular polymer foams: Progress (2004–2015) and future directions – A review. European Polymer Journal, 73, 500-519.

[108] Obi, B.E. (2018) Fundamentals of Polymeric Foams and Classification of Foam Types, Polymeric Foams Structure-Property-Performance: A Design Guide, Elsevier.

[109] Krause, B., Mettinkhof, R., van der Vegt, N. F. A.,Wessling, M. (2001) Microcellular Foaming of Amorphous High-Tg Polymers Using Carbon Dioxide. Macromolecules, 34(4), 874-884.

[110] Standau, T., Zhao, C., Murillo Castellón, S., Bonten, C.,Altstädt, V. (2019) Chemical Modification and Foam Processing of Polylactide (PLA). Polymers, 11(2), 306.

[111] Yu, L., Hao, G., Xiao, L., Yin, Q., Xia, M.,Jiang, W. (2017) Robust magnetic polystyrene foam for high efficiency and removal oil from water surface. Separation and Purification Technology, 173, 121-128.

[112] Pinto, J., Athanassiou, A.,Fragouli, D. (2016) Effect of the porous structure of polymer foams on the remediation of oil spills. Journal of Physics D: Applied Physics, 49(14), 145601.

[113] Santos, O. S. H., da Silva, M. C.,Yoshida, M. I. (2017) Synthesis and performance of different polyurethane foams as oil sorbents. Journal of Applied Polymer Science, 134(41), 45409.

[114] Laguna-Gutierrez, E., Saiz-Arroyo, C., Velasco, J. I.,Rodriguez-Perez, M. A. (2016) Low density polyethylene/silica nanocomposite foams. Relationship between chemical composition, particle dispersion, cellular structure and physical properties. European Polymer Journal, 81, 173-185.

[115] Park, C. B., Lee, P. C., Wang, J.,Padareva, V. (2006) Strategies for Achieving Microcellular LDPE Foams in Extrusion. Cellular Polymers, 25(1), 1-18.

[116] Saiz-Arroyo, C., Rodríguez-Pérez, M. Á., Velasco, J. I.,Saja, J. A. d. (2013) Influence of foaming process on the structure–properties relationship of foamed LDPE/silica nanocomposites. Composites Part B: Engineering, 48, 40-50.

[117] Sigma Aldrich, (3-aminopropyl)triethoxysilane,

https://www.sigmaaldrich.com/catalog/product/aldrich/440140?lang=en&region=TR (05.02.2020).

[118] Sigma Aldrich, (3-Glycidyloxypropyl)trimethoxysilane, https://www.sigmaaldrich.com/catalog/product/aldrich/440167?lang=en&region=TR (05.02.2020).

[119] Sigma Aldrich, Trimethoxy(octadecyl)silane, https://www.sigmaaldrich.com/catalog/product/aldrich/376213?lang=en&region=TR (05.02.2020).

[120] ASTM D1141-98 (2013) Standard Practice for the Preparation of Substitute Ocean Water, ASTM International, West Conshohocken, Pennsylvania, ABD.

[121] Suárez, M.,García-Romero, E. (2012) Variability of the surface properties of sepiolite. Applied Clay Science, 67-68, 72-82.

[122] Suárez, M., García-Rivas, J., García-Romero, E.,Jara, N. (2016) Mineralogical characterisation and surface properties of sepiolite from Polatli (Turkey). Applied Clay Science, 131, 124-130.

[123] Rajaković-Ognjanović, V., Aleksić, G.,Rajaković, L. (2008) Governing factors for motor oil removal from water with different sorption materials. Journal of Hazardous Materials, 154(1-3), 558-563.

[124] Tabak, A., Eren, E., Afsin, B.,Caglar, B. (2009) Determination of adsorptive properties of a Turkish Sepiolite for removal of Reactive Blue 15 anionic dye from aqueous solutions. Journal of Hazardous Materials, 161(2), 1087-1094.

[125] Sarı Yılmaz, M., Kalpaklı, Y.,Pişkin, S. (2013) Thermal behavior and dehydroxylation kinetics of naturally occurring sepiolite and bentonite. Journal of Thermal Analysis and Calorimetry, 114(3), 1191-1199.

[126] Inukai, K., Miyawaki, R., Tomura, S., Shimosaka, K.,Irkeç, T. (1994) Purification of Turkish sepiolite through hydrochloric acid treatment. Applied Clay Science, 9(1), 11-29.

[127] Lagashetty, A.,Abbaraju, V. (2005) Polymer nanocomposites. Resonance, 10, 49-57.

[128] Önal, M., Yilmaz, H.,Sarikaya, Y. (2008) Some physicochemical properties of the white sepiolite known as pipestone from Eskişehir, Turkey. Clays and Clay Minerals, 56(5), 511-519.

[129] Dai, J. C.,Huang, J. T. (1999) Surface modification of clays and clay–rubber composite. Applied Clay Science, 15(1), 51-65.

[130] de Lima, J. A., Camilo, F. F., Faez, R.,Cruz, S. A. (2017) A new approch to sepiolite dispersion by treatment with ionic liquids. Applied Clay Science, 143, 234-240.

[131] Yeniyol, M. (2014) Characterization of two forms of sepiolite and related Mg-rich clay minerals from Yenidoğan (Sivrihisar, Turkey). Clay Minerals, 49, 91-108.

[132] Ongen, A., Ozcan, H. K., Ozbas, E. E.,Balkaya, N. (2012) Adsorption of Astrazon Blue FGRL onto sepiolite from aqueous solutions. Desalination and Water Treatment, 40(1-3), 129-136.

[133] Cecilia, J. A., Vilarrasa-García, E., Cavalcante, C. L., Azevedo, D. C. S., Franco, F.,Rodríguez-Castellón, E. (2018) Evaluation of two fibrous clay minerals (sepiolite and palygorskite) for CO2 Capture. Journal of Environmental Chemical Engineering, 6(4), 4573-4587.

[134] Hou, K., Ouyang, J., Zheng, C., Zhang, J.,Yang, H. (2017) Surface-modified sepiolite fibers for reinforcing resin brake composites. Materials Express, 7, 104-112.

[135] Lazarević, S., Janković-Častvan, I., Jovanović, D., Milonjić, S., Janaćković, D.,Petrović, R. (2007) Adsorption of Pb2+, Cd2+ and Sr2+ ions onto natural and acid-activated sepiolites. Applied Clay Science, 37(1), 47-57.

[136] Chen, Y., Wan, C., Liu, T., Chen, Z., Qiao, Y., Lu, J., Yan, J., Zhao, L.,Esseghir, M. (2018) Evaluation of LLDPE/LDPE blend foamability by in situ rheological measurements and bubble growth simulations. Chemical Engineering Science, 192, 488-498.

[137] Eaves D. (2014) Handbook of Polymer Foams, iSmithers Rapra Publishing.

[138] Ruiz, J. A. R., Marc-Tallon, J., Pedros, M.,Dumon, M. (2011) Two-step micro cellular foaming of amorphous polymers in supercritical CO2. The Journal of Supercritical Fluids, 57(1), 87-94.

[139] Pinto, J., Escudero, J., Solórzano, E.,Rodriguez-Perez, M. A. (2018) A novel route to produce structural polymer foams with a controlled solid skin-porous core structure based on gas diffusion mechanisms. Journal of Sandwich

Structures & Materials, 22(3), 822-832.

[140] Goel, S. K.,Beckman, E. J. (1994) Generation of microcellular polymeric foams using supercritical carbon dioxide. I: Effect of pressure and temperature on nucleation. Polymer Engineering & Science, 34(14), 1137-1147.

[141] Li, H., Liu, L.,Yang, F. (2012) Hydrophobic modification of polyurethane foam for oil spill cleanup. Marine Pollution Bulletin, 64(8), 1648-1653.

[142] Songsaeng, S., Thamyongkit, P.,Poompradub, S. (2019) Natural rubber/reduced-graphene oxide composite materials: Morphological and oil adsorption properties for treatment of oil spills. Journal of Advanced Research, 20, 79-89.

[143] Wang, S., Wang, K., Pang, Y., Li, Y., Wu, F., Wang, S.,Zheng, W. (2016) Open-cell polypropylene/polyolefin elastomer blend foams fabricated for reusable oil-sorption materials. Journal of Applied Polymer Science, 133(33).

[144] Keshavarz, A., Zilouei, H., Abdolmaleki, A., Asadinezhad, A.,Nikkhah, A. A. (2016) Impregnation of polyurethane foam with activated carbon for enhancing oil removal from water. International Journal of Environmental Science and Technology, 13(2), 699-710.

[145] Santos, O. S. H., Coelho da Silva, M., Silva, V. R., Mussel, W. N.,Yoshida, M. I. (2017) Polyurethane foam impregnated with lignin as a filler for the removal of crude oil from contaminated water. Journal of Hazardous Materials, 324, 406-413.

[146] Rizvi, A., Chu, R. K. M., Lee, J. H.,Park, C. B. (2014) Superhydrophobic and Oleophilic Open-Cell Foams from Fibrillar Blends of Polypropylene and Polytetrafluoroethylene. ACS Applied Materials & Interfaces, 6(23), 21131-21140.

[147] Chawla, K. K. (1996) Interfaces in metal matrix composites. Composite Interfaces, 4(5), 287-298.

[148] Simpson, J., Hunter, S.,Aytug, T. (2015) Superhydrophobic materials and coatings: A review. Reports on progress in physics. Physical Society (Great Britain), 78, 086501.

ÖZGEÇMİŞ

KİŞİSEL BİLGİLER

Ad Soyad **:** Sinem ABALI

Doğum Yeri **:** Şişli/İstanbul

Doğum Tarihi **:** 28.02.1993

E-Mail **:** sinem_abali_93@hotmail.com

Yabancı Dil **:** İngilizce

EĞİTİM BİLGİLERİ

Lise	**:** Nişantaşı Nuri Akın Anadolu Lisesi	2007-2011
Üniversite/Bölüm	**:** Marmara Üniversitesi/Kimya Mühendisliği	2011-2017

SUNUMLAR

- Menteşoğlu Ç., Turan R., Abalı S., Aydın Y. A., (2019) Eskişehir sepiyolitinin trimetoksi(oktadesil) silan ve 3-(aminopropil)trietoksi silan ile modifikasyonu. 31. Ulusal Kimya Kongresi, 10-13 Ekim, İstanbul, Türkiye. (Poster Sunum)
- Abali S., Aydin, Y. A. (2019) Sepiolite modification by various silane coupling agents for enhanced oil uptake, 4th Eurasian Conference on Civil and Environmental Engineering (ECOCEE), 17-18 Haziran, İstanbul, Türkiye. (Sözlü Sunum)